Deutsches Zentrum
für Luft- und Raumfahrt e.V.
in der Helmholtz-Gemeinschaft

GOME / ERS-2

Level 0 to 1b ATBD

authors : Sander Slijkhuis, Bernd Aberle
document number : GOME-DLR-L1-ATBD
issue : 7.0
date : 2016-06-20
status : Rev.A

Document approval record

	digital signature	
prepared:	Sander Slijkhuis Digitally signed by Sander Slijkhuis DN: cn=Sander Slijkhuis, o=DLR, ou=MF-AP, email=sander.slijkhuis@dlr.de, c=DE Date: 2016.06.20 14:28:02 +02'00'	Bernd Aberle Digitally signed by Bernd Aberle DN: cn=Bernd Aberle, o=DLR, ou=IMF, email=bernd.aberle@dlr.de, c=DE Date: 2016.06.20 14:37:40 +02'00'
checked:		
approved PM:	Diego Loyola Digitally signed by Diego Loyola DN: c=DE, st=Bayern, o=German Aerospace Center (DLR), cn=Diego Loyola, email=Diego.Loyola@dlr.de Date: 2016.06.20 15:09:12 +02'00'	
approved CM:	Ronny Lutz Digitally signed by Ronny Lutz DN: c=DE, st=Bavaria, o=DLR, ou=IMF-ATP, cn=Ronny Lutz, email=Ronny.Lutz@dlr.de Date: 2016.06.20 15:14:39 +02'00'	

Document change record

Issue	Rev	Date	Section	Description of Change
1	A	15.9.93	all	Completely new, only polarization issues are covered
1	B	15.11.93	1.3.2, 2.5, 3.5, 4	Update of the polarisation issues after comments by A. Hahne, K. Chance and R. Spurr
2	A	18.2.94	all	Update of the polarisation issues after comments by G. Nuetzel, D. Diebel and R. Spurr, inclusion of other algorithms and rename of the document (see Document history)
2	B	6.4.94	all	Minor updates after the GSAG meetings in March and inclusion of the error calculation section (provisional)
3	A	15.7.95	all	Update of all algorithm descriptions according to the actual implementation and inclusion of new algorithms
4	A	9.8.96	all	Update of all algorithms reflecting the 1st operational version
5	B	10.04.02	all	GDP Level 0 to 1 version 2.0 (Appendix B added)
6	A	30.09.06	all	Update of algorithms reflecting GDP level 0–to–1 version 3.0 and version 4.x (latter has extractor changes)
7	A	20.06.16	all	Update of algorithms reflecting GDP level 0–to–1 version 5 ; merging with extractor SUM and rename of the document (see Document history)

Contents

1 Introduction

1.1 Purpose of the ATBD

This ATBD describes the algorithms as used for generating the “new” GOME L1b data product in NetCDF format (GDP Version 5.0). This product differs fundamentally from the “old” (GDP version 4.x and lower) proprietary GOME Level 1 data format, which basically contained Level 1a data, and where a dedicated “extraction software” tool had to be applied to obtain the fully calibrated Level 1b data that are now in the “new” product. As such, this ATBD is a merger of the previous “GOME Level 0 to 1 Algorithms Description” [G7] and the “GOME Data Processor Extraction Software User’s Manual” [G8]. The upgrade to version 5.0 has been carried out in the framework of the “GOME evolution” project.

The Global Ozone Monitoring Experiment (GOME) was originally conceived as a scaled-down version of the scanning spectrometer SCIAMACHY. It was given fast-track development status by ESA [G1], and was launched on 21 April 1995 on board the second European Remote Sensing Satellite (ERS-2). GOME provided scientific data until 4 July 2011.

GOME is a nadir-viewing spectrometer covering the range 240-790 nm in 4 spectral channels. In its normal, Earth observation mode it scans across-track in three steps. The field of view of each step may be varied in size from 40 km x 40 km to 320 km x 40 km. The mode with the largest footprint (three steps with a total swath width of 960 km x 40 km) provides global coverage at the equator within 3 days - this is the default mode of operation.

In addition to the on-line components at the ground stations, the GOME Data Processor (GDP) system [R6] is the operational off-line ground segment for GOME. The GDP was developed and implemented at DFD with the help of several scientific institutes [G2], and became operational in July 1996. It incorporates a Level 0 to 1 processing chain, the complete GOME data archive, a trace gas retrieval process (Level 1 to 2), and an image processing chain for the generation of higher-level products. The Level 1 and Level 2 data products have been generated by DFD on behalf of ESA.

1.2 Document overview

This is a merger of 2 documents (see above) with updated information on the GOME Level 0 to 1 processing.

Sections 1-3 contain document overview and references.

Section 4 provides an overview of the GOME instrument and its components.

Section 5 provides an overview of the Level 0 to 1b processing, and shows the data flow inside the processor.

Section 6 describes the algorithms used in the level 0 to 1b processing.

Limitations of the algorithms are given in Section 7.

The appendix provides a general overview of measurement errors; the specific error calculation for the Level 1b product is given in Section 6.12.

1.3 Document History

Version 7

Version 7 ATBD describes the algorithms as used for generating the “new” fully calibrated GOME L1b data product in NetCDF format, corresponding to GDP Version 5.0. This ATBD is a merger of the previous “GOME Level 0 to 1 Algorithms Description” [G7] and the “GOME Data Processor Extraction Software User’s Manual” [G8]. Algorithm updates include:

- Polarisation: for the GDF function, the O3 climatology is replaced by GOME Level 2 O3 columns from the previous GDP version (4.05).
- Dark signal correction: SAA treated as separate region
- Spectral calibration: input lamp line positions selected on basis of whole-mission stability
- Several former extraction software options are now always applied, others are no longer used for the generation of the L1b data product. See Section 5.3.4.

Version 6

Version 6 describes GDP versions 3 and 4; version 4 has updates in the GDP extraction software.

After 11 years of GOME measurements, with the instrument still in good shape, ESA has decided on the first complete Level 0–to–1 processing of the entire GOME data set. The main driver for this reprocessing has been the gaps in GDP solar calibration spectra over long time periods, caused by pointing issues on the ERS–2 platform. The new GDP (version 4.05) contains improved limit checking on solar spectra, improved line selection for better spectral calibration stability, and algorithmic changes described in the version 6 document. The precision error on the solar spectrum has been reformulated, and several options have been updated in the GDP extraction software, following the CHEOPS–GOME study [G6]. This comprises improved Peltier crosstalk correction in Band 1a, seasonal correction on BSDF, improvement in Polarisation Correction, and a new degradation correction of Earthshine Reflectivity.

Contributing Authors to version 6:

D. Loyola	DLR-MF	GOME Project Manager
B. Aberle	DLR-MF	GOME Project Engineer
A. von Bargen	former DLR-MF	former GOME Project Scientist
W. Balzer	DLR-MF	former GOME Project Manager
E. Hegels	former DLR-MF	former GOME Project Scientist
S. Slijkhuis	DLR-MF	GOME Project Scientist
R. Spurr	now R. T. Solutions	former GOME Project Scientist

Version 5 and lower

The first issue of the document was released in September 1993; the second issue was written to include updated polarisation correction algorithm description and error calculations. The third issue (July 1995) updated the algorithm descriptions in the light of the first operational trials following the successful launch of the ERS–2 satellite in April 1995. After the instrument commissioning phase, the data processing validation campaign took place in the period October 1995 to March 1996, followed by a three–month period of analysis and trouble–shooting. In July 1996 the GDP 0–1 system reached a plateau, with the first public release of level 2 products scheduled for August 1996, and the first public release of Level 1 data planned for January 1997 following further improvements in key data and 0–1 algorithms..

At the final meeting of the ”Tiger Team” validation group at DLR on June 24/25 1996, a high priority recommendation was made to update GDP documentation. The 4th Issue of the Level 0 to 1 Algorithms Description Technical Note is one of the main outcomes of this recommendation.

Version 5 described improved cross–correlation, the degradation of the BSDF, and the degradation of the measurement channels.

1.4 Acknowledgements

The authors would like to thank the following people working on algorithm and processor development, providing useful discussions, and performing the internal review of this document:

- Melanie Coldewey-Egbers
- Angelika Dehn (ESA)
- Gabriele Brizzi (ESA)

We thank Nathalie Nicastro for great assistance with reformatting the formulae.

2 Applicable and reference documents

2.1 Applicable documents

[AD1] GOME In–flight Calibration and Characterisation Plan, ER–PL–ESA–GO–0303, Issue 1/–, August 93

2.2 Reference documents

[R1] Hiroshi Akima, "A new method of interpolation and smooth curve fitting based on local procedures", J. ACM, Vol. 17(4), 589-602, 1970

[R2] Data Reduction from Experimental Histograms, W.R. Falk (University of Manitoba, Winnipeg, Canada), Nuclear Instruments and Methods in Physics Research 220**,** p. 473-478, 1984

[R3] William H. Press et al., "Numerical Recipes in C", Cambridge University Press, 1994

[R4] Jochen Stutz and Ulrich Platt, "Problems in using diode arrays for open path DOAS measurements of atmospheric species", Proc. SPIE Vol.1715 p.327, 1993

[R5] P. Stammes, "The seventh point polarisation algorithm, Internal Report" (GOME and SCIAMACHY), KNMI De Bilt, 1994

[R6] D.Loyola, W.Balzer, B.Aberle, M.Bittner, K.Kretschel, E.Mikusch, H.Muehle, T.Ruppert, C.Schmid, S.Slijkhuis, R.Spurr, W.Thomas, T.Wieland, M.Wolfmueller, "Ground segment for ERS-2 GOME sensor at the German D-PAF", Proceedings of the Third ERS Symposium on "Space at the Service of our Environment", ESA SP-414, Vol. II, 591-596, Florence 1997

[R7] P. Stammes, I. Aben, R.B.A. Koelemeijer, S. Slijkhuis, D.M. Stam, "GOME polarisation validation study", Proceedings of the Third ERS Symposium on "Space at the Service of our Environment", ESA SP-414, Vol. II, 669-674, Florence 1997

[R8] K. Bramsted, M. Weber, J. Burrows (IFE/IUP univ. Bremen), "Radiance Jumps and PMDs in GOME", GOME workshop 24.06.1996

[R9] C. Caspar, "GOME Dark Signal Characterisation", ER-TN-ESA-GO-0473, draft issue 1.0, 06.11.1995

[R10] Hegels E., "ERS-2/GOME - Support, Progress Report", ER-TN-DLR-GO-0044, Issue 1, 29.1.1999.

[R11] Aben I., C. Tanzi, E. Hegels and M. Eisinger, "GDAQI - GOME Data Quality Improvement", TN-GDAQI-001SR/99, Midterm report, Draft, April 1999.

[R12] Burrows, J.P. et al., “The Global Ozone Monitoring Experiment (GOME): Mission Concept and First Scientific Results”, J. Atmos. Sci. 56, 151-175, 1999

[R13] SCIAMACHY Level 0 to 1c Processing - Algorithm Theoretical Basis Document, ENV-ATB-DLR-SCIA-0041, Issue 2, DLR, 14.12.2001

[R14] Slijkhuis, S., "CHEOPS-GOME Study on seasonal effects on the ERS-2/GOME Diffuser BSDF", DLR report CH-TN-DLR-GO-0001, Issue 1, May 2004

[R15] S. Slijkhuis, "Study on Correction of Signal Background on the ERS-2/GOME Level 1 data", DLR report CH-TN-DLR-GO-0002, Issue 1, 3.9.2004

[R16] Krijger, J.M., Aben, I., Landgraf, J.,: CHEOPS-GOME: WP2.1: Study of Instrument Degradation, ESA SRON-EOS/RP/05-018 Tech. rep., 2005

[R17] J.M. Krijger, I Aben, J. Landgraf, "GOME: scan-mirror degradation correction", Proc. ESA First Atmospheric Science Conference , May 2006, ESA SP-628 cd-rom

[R18] M. Coldewey-Egbers, S.Slijkhuis, B.Aberle, D.Loyola: Long-term analysis of GOME in-flight calibration parameters and instrument degradation, Applied Optics 47, p.4749, 2008

[R19] HDF5, Release 1, The National Center of Supercomputing Applications at the University of Illinois, Urbana-Champaign, IL, 1998

[R20] N.A.J. Schutgens, P. Stammes, "Parametrisation of earth's polarisation spectrum from 290 to 330 nm", J.Quant.Spectr.Rad.Transf. 75, p.239, 2002

[R21] J.H.G.M. van Geffen, "Documentation of the software package GomeCal (Version 1.0)", KNMI Technical Report TR-255, 2003

[R22] Fortuin, J.P.F. and Kelder, H.M."An ozone climatology based on ozone sonde and satellite measurements," J. Geophys. Res. 103, p.31,709, 1998

[R23] S. Slijkhuis , B. Aberle , M. Coldewey-Egbers, D. Loyola, A. Dehn, T. Fehr, "GOME/ERS-2: New homogeneous Level 1b data from an old instrument", Proc. ESA ATMOS2015, ESA SP-735, P72, November 2015

2.3 GOME Project Documentation

[G1] GOME Interim Science Report, edited by T. D. Guyenne and C. J. Readings, SP-1151, ESA publications Division, ESTEC, Noordwijk NL, ISBN 92-9092-041-6 (1993)

[G2] GOME Users Manual, ESA SP-1182, ESA/ESTEC, Noordwijk, The Netherlands (1996)

[G3] GOME BBM Calibration Results Review II Data Package, Issue 1, 9.3.1994

[G4] GOME FM Calibration Results Review Data Package, Issue 1, 14.11.1994

[G5] Product Specification Document of the GOME data processor, ER-TN-DLR-GO-0016, Iss./Rev. 5/A, March 2009 (the latest version is included on the product FTP-site)

[G6] CHEOPS-GOME ATBD Level 0 to 1 Processing Update, CH-TN-DLR-GO-0003, Issue 1/B, 05.06.2006

[G7] GOME Level 0 to 1b Algorithm Description, ER-TN-DLR-GO-0022, Issue 6/A, 09.2006.

[G8] GOME Data Processor Extraction Software Users's Manual, ER-SUM-DLR-GO-0045, Issue 4, 17.03..2009.

2.4 Selected Online material

[W1] Instrument and science overview: http://www.iup.uni-bremen.de/gome/

[W2] ERS mission overview: https://directory.eoportal.org/web/eoportal/satellite-missions/e/ers-2

[W3] GOME product info: http://atmos.eoc.dlr.de/gome/documentation.html

[W4] GOME web gallery: https://earth.esa.int/web/sppa/ (URL TBC)

3 Terms, definitions and abbreviations

3.1 Terms and definitions

Band (spectral-)
one of 4 (or 6) spectral bands referring to parts of an array detector:
band 1a and 1b cover the short-wavelength and long-wavelength part of channel 1 respectively,
band 2a and 2b cover the short-wavelength and long-wavelength part of channel 2,
band 3 and 4 are identical to channel 3 and 4.
In addition there are 4 ‘straylight’ bands: two shortwave of band 1a, one longwave of band 1b, and one shortwave of band 2a. These ‘straylight’ bands are not part of the standard level 1 extracted data, but they are available on the level 1 product.

Channel
one of the 4 spectral channels containing an array detector, sometimes an expression like ‘channel 1a’ is used for ‘band 1a’ etc.

Data Packet
one unit of scientific instrument data; generated every 1.5 second

Extractor
a software tool to inflate a Level 1 Product into fully calibrated Level 1 Data (no longer used since version 5).

FPA crosstalk
a phenomenon which may cause a variation in detector signal related to the switching of coolers for the Focal Plane Assembly (detector housing).

Ground pixel
the footprint on the Earth’s surface during one integration time.

Integration time pattern
specifies the integration time of each of the 6 bands

Level 1b Product
a data set (usually 1 orbit or a subset thereof) which contains the fully calibrated GOME (ir)radiance spectra.

Pixel
usually one spectral element on the detector is meant; depending on the context this may also be shorthand for ‘ground pixel’.

Pixel (sub-)type
denotes a certain geometry in the scan pattern; pixel type 0,1,2,3 refer to the East, Nadir, West and Backscan ground pixel, respectively.

Virtual pixel
a wavelength interval on the PMD detector which corresponds to the wavelength interval of the corresponding channel array detector pixel.

Virtual channel boundary
the pixel or wavelength which separates band 1a from 1b (or 2a from 2b); this can be set by macro-command from the ground operator.

3.2 Acronyms and abbreviations

AMF	Air Mass Factor
ATBD	Algorithm Theoretical Basis Document
ATSR	Along-Track Scanning Radiometer
BBM	Breadboard Model
BOA	Bottom of Atmosphere
BSDF	Bi–directional Scattering Distribution Function
CU	Calibration Unit
DLR	German Aerospace Center (Deutsches Zentrum für Luft- und Raumfahrt)
DFD	German Remote Sensing Data Centre
DOAS	Differential Optical Absorption Spectroscopy
DP	Data Packet
DU	Dobson Unit
ENVISAT	Environmental Satellite
EO	Earth Observation
ERS-2	European Remote Sensing Satellite-2
ESA	European Space Agency
ESOC	European Space Operation Centre
ESTEC	European Space Centre of Technology
ESRIN	European Space Research Institute
FM	Flight Model
FWHM	Full Width at Half Maximum
FSM	Flight Spare Model
GDF	General Distribution Function (for UV polarisation)
GDP	GOME Data Processor
GOME	Global Ozone Monitoring Experiment
HK	Housekeeping (Data)
ISRF	Instrument Spectral Response Function (“slit function”)
LED	Light Emitting Diode
hPa	Hectopascals
IFE	Institute of Environmental Physics, Bremen University
IMF	Institut für Methodik der Fernerkundung (DLR)
KNMI	Koninklijk Nederlands Meteorologisch Instituut
LIDORT	LInearised Discrete Ordinate Radiative Transfer
LBL	Line-by-Line
LUT	Look Up Table
MetOp	Meteorological Operational
MLER	Minimum Lambert equivalent Reflectivity
MSG	Meteosat Second Generation
MRTD	Mission Requirements Traceability Document
MODIS	Moderate Resolution Imaging Spectroradiometer
NASA	National Aeronautics and Space Administration
NetCDF-CF	Network Common Data Format – Climate and Forecast (CF) convention
NIR	Near Infra-Red
NPP	NPOESS Preparatory Project (NASA platform)

NRT	Near-Real-Time
OFL	Off-line
OMI	Ozone Monitoring Instrument
PMD	Polarization Measurement Device
QE	Quantum Efficiency
RGB	Red-Green-Blue
RMS	Root-Mean-Square
RT	Radiative Transfer
ROCINN	Retrieval of Cloud Information using Neural Networks
SAA	South Atlantic Anomaly
SCIAMACHY	SCanning Imaging Absorption spectroMeter for Atmospheric CartograpHY
SGP	SCIAMACHY Ground Processor
SLS	Spectral Line Source (GOME calibration lamp)
SMR	Sun Mean Reference
SRD	Systems Requirement Document
SRON	Netherlands Institute for Space Research
SZA	Solar Zenith Angle
TOA	Top of Atmosphere
TOMS	Total Ozone Mapping Spectrometer
TPD/TNO	Netherlands Organisation for Applied Scientific Research
UPAS	Universal Processor for UV/VIS Atmospheric Spectrometers
UV	Ultra Violet
VCD	Vertical Column Density
VIS	Visible
VLIDORT	Vector LInearised Discrete Ordinate Radiative Transfer

4 Overview of the instrument and its operation

A detailed overview of the instrument, its operation, and scientific methods, has been given in the GOME User's manual [G2]. That document also contains detailed drawings and photographs of various parts of the instrument. Information may also be found in e.g. Burrows et al.1999 [R12]. Some online information is available in e.g. [W1], [W2]. See also the GOME web gallery [W4].

For understanding the algorithm principles we will here present a more schematic overview. A high-level view of the relevant functional blocks of the instrument is shown in Figure 4-1.

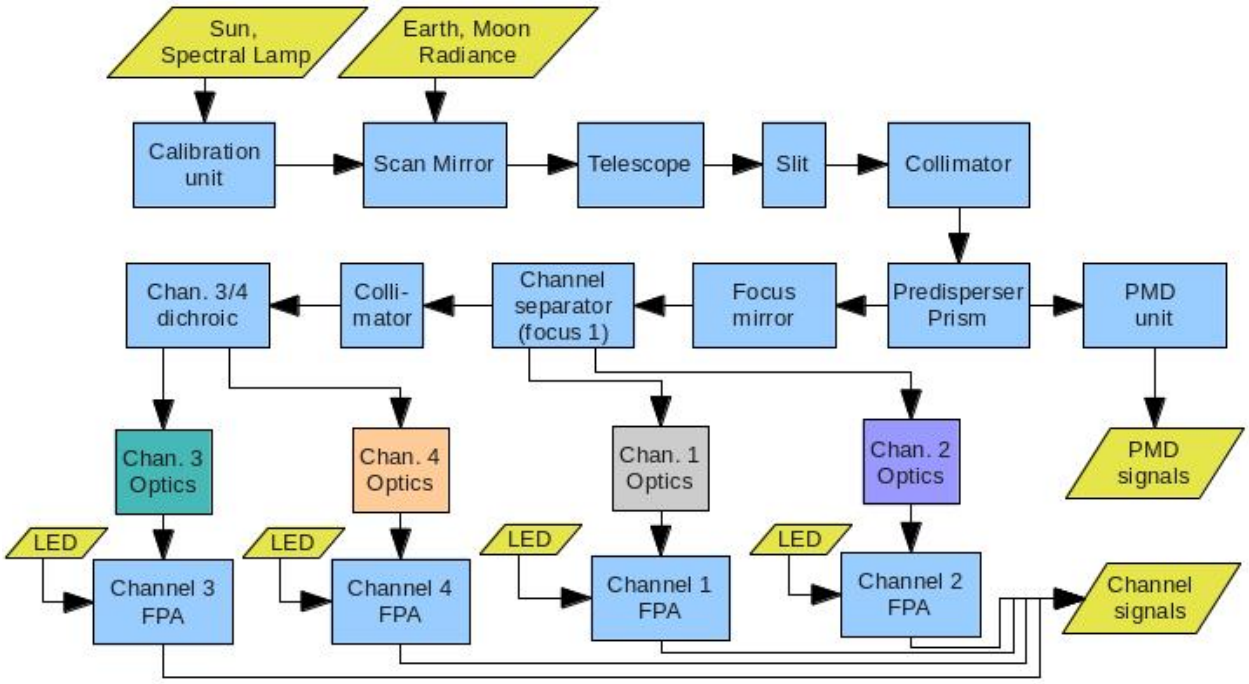

Figure 4-1 Functional diagram of the GOME instrument

The GOME instrument is designed as double spectrometer. At an intermediate focal plane a spatial filter separates the wavelengths for channel 1 (UV), for channel 2 (near-UV), and for channel 3+4 (visible / NIR). This early separation serves to reduce straylight on the UV detectors, since the Earth radiance at visible wavelengths is up to a factor ~1000 larger than the UV radiance. After re-collimation, the light is dispersed in each channel by gratings and focused again on the detectors in the focal plane assembly (FPA) in each channel.

In the following we discuss some of the instrument components that are relevant to the Level 0 to 1b processing.

Scan mirror

The position of the scan mirror is linked to the observation mode.

For radiance observations we have the following positions

- nadir pointing (also called "static")
- nadir scanning – viewing angle scanning around Nadir. The default scan range is between -30° ("East") and +30° ("West") around nadir (mirror angle ±15°) which yields a swath of 960 km width on the ground, but on a regular basis also a "narrow swath" of 360 km has been made.
- pole scanning: as nadir scanning, but around the pole view position. Pole view is pointing to North Pole at 47.62 ° or pointing to South Pole at -47.62 °

- Moon view: scan mirror looking “West” above the Earth’s Limb with a viewing angle between +70 and +85 degree

For dark signal measurements, which are executed in each eclipse phase of the orbit, the scan mirror looks inside the instrument towards the telescope optics.

For Sun calibration or for Spectral calibration, the scan mirror may look at one of several mirrors within the calibration unit (depending on which source is selected, see below).

The scan mirror is the optical element that is most exposed to contamination from outside, and it also receives the highest UV dose of any optical surface. Therefore, it is the optical element that is most prone to degradation of the transmission. In principle, this degradation is scan angle dependent, and also the polarisation properties are expected to change in case of degradation. However, the GOME instrument provides no direct way to measure such changes. In level 0 to 1b processing, only the transmission function for the Sun observation angle is corrected.

Calibration Unit

The Calibration Unit (CU) hosts the spectral calibration lamp, the Sun Diffuser, and some mirrors to direct the various light beams to the scan mirror.

The hollow cathode lamp is filled with Neon and has a Pt/Cr alloy electrode, thus providing atomic lines of these three elements. The lamp is located behind a transmission diffuser, which generates a broad light beam. Part of this beam is [always] split off and directed over the Sun Diffuser. The scan mirror may either look at the “direct” beam, or at the one over the Sun Diffuser. Comparison of the two enables to derive the degradation of the Sun diffuser over the instrument’s lifetime. The lamp has a limited lifetime [burning time / switches], and near the end of the mission the frequency of spectral lamp measurements was reduced.

The Sun Diffuser is located behind a port which looks in the horizontal plane through the flight direction. The centre position of the field of view is 22^{o} East of the flight direction. The port is closed by a shutter most of the time, but when the instrument comes out of eclipse, the shutter may be opened to observe the rising Sun (by default, this is done once per day).

Since the instrument moves towards the Sun, the solar calibration spectrum is Doppler-shifted. In contrast, the radiance measurements are not Doppler-shifted, because the viewing angle is perpendicular to the flight direction.

During the time that the Sun is visible, the Sunlight moves in the elevation direction over the Diffuser [$\pm 1.5^{o}$]. During one observation, the solar azimuth remains constant. However, this azimuth direction may vary by $\pm 8^{o}$ during the year (similar to the Analemma).

The Diffuser BSDF is sensitive to both, elevation and azimuth angle. A drawback of the ground aluminium surface diffuser used in GOME, is that the BSDF is not smooth but shows a “speckle” effect. The speckle effect cannot be corrected in level 0 to 1b processing, but the effect is reduced by averaging all solar spectra [at different elevation] taken during one observation.

Slit

The slit limits the instantaneous field of view to 2.9^{o} x 0.142^{o} or 40 x 2 km on the ground. Note that a default scan lasts 4 x 1.5 = 6 seconds (3 exposures in forward direction and 1 exposure during the backscan) in which time the spacecraft moves 40 km. We thus get a scanning pattern as depicted in Figure 4-2, with continuous ground coverage in successive forward scans.

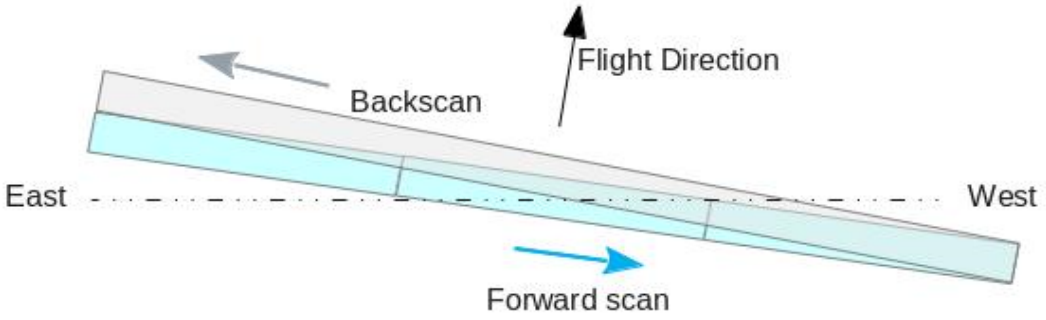

Figure 4-2 GOME scan pattern with 3 readouts of 1.5 second in forward scan and 1 readout of 1.5 second in backscan (East/West indicated for descending part of orbit)

Note that for Moon observations, the slit cuts out a slice of the Lunar disk (depending on Moon phase), while the Moon's 0.5^{o} diameter does not fill the length of the slit. This makes a radiometric calibration of the Moon's radiance difficult, also because the Moonlight is polarised (depending on phase and surface reflectance). Level 0 to 1b processing will therefore not attempt to generate calibrated radiances for the Moon.

The instrument's resolution is partially determined by the width of the slit as projected on the detector pixels. The "Slit Function" or ISRF, i.e. the instrument spectral response to monochromatic input, is a convolution of projected slit width, pixel response, and optical abberations. In GOME, the optical abberations are a significant part of the slit function, especially at the detector edges. This is insofar favourable, as that any intensity gradient across the slit width is smeared out. Therefore, GOME is relatively insensitive to the effect of non-homogeneous scene illumination.

Predisperser prism

The light beam from the telescope collimator goes through a quartz prism, where it strikes the back surface at the Brewster angle. This causes a part of the light, polarised parallel to the slit, to be back-reflected and then directed towards the PMD unit (see below). The remainder of the beam (which is then more polarised perpendicular to the slit) goes forth towards the channel separator.

The light (both for channels and PMDs) is dispersed by the prism. The amount of dispersion (governed by the refractive index of the prism) depends on the prism's temperature. This temperature is in fact the dominant factor for spectral shifts. For this reason, level 0 to 1 processing will assign spectral calibration data as function of the temperature from a sensor near the predisperser prism.

Channel separator

The pre-dispersed light is focussed into an intermediate spectrum. In this focal plane, a partially aluminised prism covers the UV part of the spectrum. While the visible/NIR light (for channels 3 and 4) goes past this channel separator prism, the light for channel 2 is reflected by the aluminised surface., The light for channel 1 goes through the non-aluminised part of the prism and undergoes an internal reflection (since input and output direction are perpendicular to a prism surface, this doesn't cause additional dispersion).

The spectrum has very low resolution on the channel separator. Therefore, wavelength separation is not abrupt, but spectral overlap arises at the extreme wavelengths in each channel. Originally it was planned to use this overlap in the determination of atmospheric polarisation (next to information from the PMDs), since different channels have a different sensitivity to polarisation. However, it has turned out that other effects (e.g. beam inhomogeneity) have an influence on the amount of light assigned to each channel. Therefore, the overlaps are no longer used in level 0 to 1 processing.

Dichroic

The dichroic filter separates the wavelengths of channel 3 from those of channel 4. In the wavelength range from ~590 to ~610 nm the filter changes from reflection to transmission. Here we have a spectral overlap between channel 3 and 4. In the overlap, the instrument response depends very strongly on polarisation (the transmission curve shifts in wavelength, depending on polarisation angle). Outside the overlap region, the filter's transmission curve is slightly dependent on polarisation angle [G2].

It appeared that the transmission curve of the dichroic changed significantly from ground to in-flight, and also during the first months in space; probably due to outgassing of the filter coatings. Afterwards the changes were less, but the dichroic was not completely stable. The resulting "dichroic features" in the instrument response are particularly visible in the channel overlap region and in the region 450-480 nm (see also Figure 5-1).

Channel optics

The channel optics consist of 4 quartz lenses mounted in one barrel. The barrel is made of titanium, to minimize focal shifts with temperature (the GOME optics are not temperature-stabilised). There is some spectral smile (wavelength shift as function of slit height), especially at the short-wavelength end of Channel 2. This is not directly observable because the slit height is not resolved in pixels (each pixel in the linear detector array covers the complete slit). However, smile might cause small wavelength shifts or change in slit function FWHM when only part of the slit is illuminated (as e.g. in Moon measurements or in partially clouded scenes).

LEDs

Each channel has a red LED, located between the channel optics and the detector window. Thus, the LEDs illuminate the detectors without any influence of [degradation of] the optics. The LEDs may be used for characterising the pixel-to-pixel sensitivity (PPG) of the detector. However, the quantum efficiency of detector pixels varies with wavelength and this wavelength curve is not necessarily exactly the same for all pixels. Especially in the UV the determination of PPG from red LEDs is not necessarily exact (since we measure PPG for red light but need PPG for UV light). On the other hand, the pixels of the Reticon linear array detectors are very large, and thus relative changes in pixel size (thought to be the main cause of PPG) are expected to be small. Indeed, the PPG is in practice very small (order of 0.001), such that the errors due to wavelength-dependent QE are considered tolerable.

FPAs

The Focal Plane Assembly in each channel holds the Reticon detector and the pre-amplifier electronics. A Peltier cooler stabilises the detector temperature on -38^{o}C to reduce dark current. It appeared that switches in the Peltier cooling introduced electronic crosstalk. The Level 0 to 1b processing mitigates these effects.

The Reticons are linear arrays with 1024 pixels of 25 µm x 2500 µm, which are read out sequentially. This has the effect, that the ground scene covered by the last detector pixel is shifted a bit w.r.t. the first detector pixel (because the instrument scans and flies further during readout). The readout time of the total array lasts 0.09375 seconds. Although this is still small compared to the nominal integration time of 1.5s, effects are visible in the data when scanning strongly inhomogeneous scenes; in particular that may show up as discontinuities in channel overlaps (since the reading start of the longer-wavelength channel is compared to the reading end of the shorter-wavelength channel). See also the discussion on "radiance jumps" in Section 6.10. The pixels are read out in reverse order as they appear on the Level 0 product, thus pixel 1023 is read out first.

Electronically, the Reticons for channel 1 and 2 are separated in 2 bands, which may be read out after a different exposure time. These bands are denoted 1a, 1b and 2a, 2b respectively.

The detector surface is protected with a 3 µm thick SiO_2 coating. This causes an interference pattern called Etalon [R4] that normally may be calibrated out. Unfortunately, changing deposits (“ice”) on the detectors have caused this etalon structure to shift in-flight.

PMD Unit

GOME has three “Polarisation Measurement Devices” (PMDs). These are photodiodes which are sampled at a frequency of 16 times per 1.5 second (the latter being the nominal channel integration time). Each photodiode is coupled to an RC circuit, which acts as a smoothing filter to “integrate” the signal over a time roughly equal to the sampling time.

The PMD detectors are located behind a focussing mirror, which receives the light beam that is split off from the pre-disperser prism. As mentioned above, this light is almost completely polarised in a direction parallel to the instrument slit. Since no polarisation mixing occurs inside GOME (see also Section 6.11.1), the PMDs thus measure the parallel polarised component of the atmospheric radiance.

The spectral bandwidth of PMD 1, 2, 3 corresponds roughly to the detector array channels 2, 3, 4, respectively. However, they extend somewhat into neighbouring channels. PMD 3 also extends beyond the upper wavelength range of the GOME channel 4.

5 Overview of Level 0 to 1b processing

5.1 Calibration approach

5.1.1 Basic equations

The generic expression for the signal detected by each detector pixel, as function of the incident radiation and as function of the instrument characteristics, can be written as:

$$S_i = I(\lambda_i) \cdot T(\lambda_i) \cdot Q_i + SS_i + DS_i \qquad \text{Eq.(5-1)}$$

with

- S_i measured signal at detector pixel i
- λ_i wavelength of detector pixel i
- $I(\lambda_i)$ incident radiation as function of wavelength
- $T(\lambda_i)$ optical transmission function of instrument as function of wavelength
- Q_i detector efficiency (including conversion to 'binary units') of detector pixel i
- SS_i straylight signal at detector pixel i (depending on all signals in the channel)
- DS_i dark signal of detector pixel i

where it is assumed that the detector and electronics respond linearly to input signal. Non-linearities have not been found for GOME, except close to detector saturation. In Level 1b, signals in the non-linear regime are flagged as saturated, above a limit of 53,000-58,000 BU.

Inverting Eq.(5-1) yields the expression for the retrieved atmospheric intensity (on the Level 1b product given in units of photons/(s.cm2.sr.nm) for Earth-shine measurements c.q. photons/(s.cm2.nm) for the Sun measurements):

$$I(\lambda_i) = \frac{S_i - SS_i - DS_i}{T(\lambda_i) \cdot Q_i} \qquad \text{Eq.(5-2)}$$

Instrument calibration comprises the determination of all quantities (except S_i) in the right-hand side of this equation. The quantities in the denominator deserve special attention, since they are in practice varying with time due to:

- wavelength shifts
- general degradation of the optics
- degradation of detector pixels
- varying interference patterns on detector (e.g. build-up of thin ice layers).

The latter issue is called Etaloning [R4]. The changes in etalon manifest themselves as a changing wave pattern, with typically 5-10 waves per GOME channel. Unfortunately, GOME has no on-board calibration source suited to characterise this pattern reliably. Therefore, Level 1b will not attempt to correct these variations (see also Section 5.1.5).

When correcting the "Radiance Response" function of the instrument, $T(\lambda_i) \cdot Q_i$, for wavelength shifts, we encounter the problem that only its wavelength-dependent part must be shifted and not its pixel-dependent part (the wavelength-dependent part is formed by the transmission of the optics and the quantum efficiency of the detector material; the pixel-dependent part is formed by pixel geometrical size and possible radiation damage to pixels). This separation into a wavelength- and a pixel-dependent part is difficult to make since in practice only the end-to-end throughput is measured.

The usual approach is to postulate that the wavelength-dependent part is a smooth function of wavelength. The radiance response function is smoothed with a certain filter and this is taken as its wavelength-dependent part; the remaining structure on a pixel-to-pixel scale is

taken as the pixel-dependent part. However, there is a certain arbitrariness in this approach by the choice of the smoothing filter.

The pixel-dependent part of the radiance response function, called pixel-to-pixel gain (PPG) is determined by illuminating the detector with a light source with a smooth spectrum. To this end, each GOME channel has a (red) LED in front of the detector assembly – the LED illuminates the detector while bypassing all optical elements.

Changes in instrument response function other than etalon and PPG are usually caused by a gradual degradation in optics or electronics. This degradation must be monitored by scientific analysis of the data set. Such changes in instrument response may be accounted for in the calibration equation accounted for via so-called “degradation correction” factors.

An additional complication for GOME calibration is that the instrument response function depends on the polarisation state of the incoming light – the main polarisation-sensitive optical elements are pre-disperser prism, gratings and the dichroic; but also the scan mirror is polarisation sensitive. In GOME calibration, this is implemented as a polarisation correction factor, applied to the response function measured for unpolarised light. The polarisation state of the incoming light is determined for each measured channel signal, using the PMD-detector measurements recorded during the integration time of the channel signal.

Taking all of the above effects into account, we can rewrite the generic calibration equation as:

$$I(\lambda_i) = \frac{S_i - SS_i - DS_i}{c_{pol}(\lambda_i, p_t(\lambda_i)) \cdot (R_{0,i}/PPG_{0,i})(\lambda_i) \cdot PPG_{t,i}(\lambda_i) \cdot m_t(\lambda_i) \cdot E_t(\lambda_i)} \qquad \text{Eq.(5-3)}$$

where subscript 0 denotes the quantity at a reference time t = 0 and subscript t denotes the quantity at the time of measurement, and

$(R_{0,i}/PPG_{0,i})(\lambda_i)$	smooth part of the radiance response function as function of wavelength, for unpolarised input
$c_{pol}(\lambda_i, p_t(\lambda_i))$	polarisation correction factor as function of wavelength and input polarisation
$PPG_{t,i}(\lambda_i)$	pixel-to-pixel part of response function at detector pixel i
$m_t(\lambda_i)$	degradation monitoring factor as function of wavelength
$E_t(\lambda_i)$	etalon change as function of wavelength

The above equation is valid for the atmospheric measurements. For the observation of the Sun there is additionally a diffuser plate (plus auxiliary optics) in the light path. The scattering properties of the diffuser plate depend both on the elevation angle of the incident beam (which is a function of time in the orbit) and on its azimuth angle (which is a function of time of the year); this 2-dimensional dependency is expressed in the bi-directional scattering function (BSDF) of the diffuser. Noting that the sunlight is unpolarised, the generic calibration equation then takes the form:

$$I(\lambda_i) = \frac{S_i - SS_i - DS_i}{BSDF_0(\lambda_i) \cdot m_{BSDF,t}(\lambda_i) \cdot (R_{0,i}/PPG_{0,i})(\lambda_i) \cdot PPG_{t,i}(\lambda_i) \cdot m_t(\lambda_i) \cdot E_t(\lambda_i)} \qquad \text{Eq.(5-4)}$$

5.1.2 Overview of Calibration Procedures

Calibration of the instrument is performed on 3 different levels:

1. On-ground Calibration:

determines the instrument response to calibrated radiance and irradiance sources as function of wavelength and scan mirror angles; determines the straylight properties of the instrument; provides preliminary calibration of wavelength and dark signal.

2. Level 0 to 1b Processing of Calibration Constants:
   Calibration constants which can be directly derived from measurements using on-board calibration sources are determined during the operational Level 0 to 1 processing. This comprises dark signal measurements on the night side of each orbit, and at regular intervals wavelength calibration using the spectral lamp measurements and PPG calibration using the LED measurements.
3. Correction of degradation:
   due to degradation in optical components or detectors, the calibration constants for radiance and irradiance will change in time. This degradation cannot be derived from on-board calibration sources and has to be modelled externally from the data processor. For the GOME Level 1b product, this has been done by scientific analysis of time sequences of solar observations.

5.1.3 On-ground Calibration

The on-ground calibration has been performed by TPD/TNO. The output of the on-ground calibration relevant to the operational Level 0 to 1 processing, is a data set containing the so-called '***Calibration Key Data***'.

For various reasons the original Key Data set had to be adjusted from the on-ground situation to the in-flight situation; mostly due to air-vacuum wavelength shifts and outgassing of optical coatings. This has resulted in several updates of the Key Data set by TPD (up to Version 8). Using time series of several years, further adjustments have been made by SRON and DLR to the radiance response keydata (spectral features only, not absolute levels) [R10][R11] and to the diffuser BSDF [R11][R14].

The current Version 8.40 of the keydata file, named "PRE_FLIG", contains the following parameters (for an explanation see Section 6):

```
**      Relative Error Budget on KeyData Functions
**      Uniform Straylight Level
**      Straylight Ghost Characteristics
**      Out of Band Straylight PMD's Correction
**      Spectral Calibration Lines
**      Scale Factors for FPA Correction
**      Number of FPA Filter Coefficients Used
**      Filter Coefficients for FPA Correction
**      BSDF Bi-directional Scattering Distribution Function Coefficients
**      Radiance Response
**      Radiance Scan Mirror Dependency Factor Angles
**      Radiance Scan Mirror Dependency Factor for Channel 1 to 4
**      Radiance Overlap Correction Function f2 Temperatures
**      Radiance Overlap Correction Function f2 for Channel 1 to 4
**      Eta_Nadir Polarization Sensitivity Ratio
**      Chi Polarization Sensitivity Correction Factor Angles
**      Chi Polarization Sensitivity Correction Factor for Channel 1 to 4
**      Ksi Polarization Sensitivity Ratio of PMD 1,2,3
```

5.1.4 Level 0 to 1 Processing of in-flight Calibration Constants

Dark signal from the channel array detectors and from the PMDs is measured at each dark side of the orbit. Dark signal has a fixed component, the so-called fixed-pattern noise (FPN), as well as a component due to charge leaking which increases linearly with detector exposure time. Therefore, a series of dark spectra is taken at each night side of the orbit. All integration time patterns (i.e. combinations of IT for the different detectors) which may occur in the science measurement are covered. The dark spectra are included in a Calibration

Database as function of integration time pattern. For processing, the most recent applicable dark spectrum from the database is used.

Spectral calibration is performed at regular intervals (typically monthly) using the sharp emission lines of an internal Pt/Cr-Ne hollow cathode lamp (the SLS). For each channel, a 3rd order (in channels 1,2) or 4th order (in channels 3,4) polynomial is fitted to the spectral line positions to obtain wavelength as a function of pixel number.

The wavelength calibration depends on the temperature of the optical bench. Therefore the polynomial calibration constants are stored in the Calibration Database as function of temperature. For processing, the most recent applicable coefficients from the database are used. The typical temperature variation over one orbit is ~1 K; the instrument starts heating up as soon as it enters sunlight and it starts to cool down when entering the dark part of the orbit.

Calibration measurements from Light Emitting Diodes (LEDs), which are placed close to the detectors, are used for flat-fielding the spectra of each detector array. This comprises the calculation of pixel-to-pixel gain (PPG). The PPG calibration is also done only at regular (typically monthly) intervals.

Daily observations of the Sun over a diffuser plate provides a solar reference which is used in the calculation of the Earth-shine reflectivity spectra. The calibrated solar irradiance spectrum is output as measurement data on the product of the orbit containing the solar measurement; for subsequent orbits it is used as calibration data for reflectivity, until a new Sun is observed. This calibration data is referred to as the “Sun Mean Reference” (SMR).

5.1.5 Correction for degradation

The degradation of the instrument may be monitored by combining measurements from several sources over a longer period in time. This is an off-line activity. The results are fed into the data processor as additional calibration constants.

For the operational Level 0 to 1b processor, instrument degradation has been primarily derived from Sun measurements. An important issue is the separation of [degradation in] Diffuser BSDF from the Radiance Response function. Measurements of the SLS over the Diffuser have shown that Diffuser degradation is minimal – this degradation has then been neglected. However, seasonally repeating patterns in instrument degradation showed that there was still an issue with uncorrected azimuth dependency of the diffuser BSDF. Earlier analysis results have been reported in [R10][R11], where the degradation observed in Sun measurements was simultaneous fitted with a correction factor for solar azimuth and a degradation function. After a more accurate determination of the BSDF’s azimuth dependency [R14], the current degradation correction only fits the radiance response function, using a polynomial wavelength dependence with temporal Savitzky-Golay smoothing (see also [R23]).

At present no attempts are being made to correct for the etalon effect - a low-frequency spatial (i.e. as function of pixel number) oscillation in detector response caused by a changing thickness of ice deposits on the detector (see e.g. [R4]). For level 1 to 2 processing using the DOAS spectral analysis method this effect is not significant, since it divides out of the ratio of earth-shine to solar spectra.

For illustration, Figure 5-1 shows a yearly snapshot of the degradation seen in the Sun measurements. Solar data from the same day in each year are used to divide out any effects of changing solar incidence angle on the diffuser. The loss in throughput is especially severe in channel 1: after 2004 less than 25% of throughput remained below 300 nm. This implies a significant deterioration in signal-to-noise. The wave structures seen on the spectral ratios are due to change in etalon. In the figure, two spectral regions around 470 nm and 600 nm are marked with a yellow bar. In these regions we observe unpredictable polarisation-sensitive changes which are associated to changes [outgassing] in the dichroic filter. The radiometric calibration in these regions cannot be trusted.

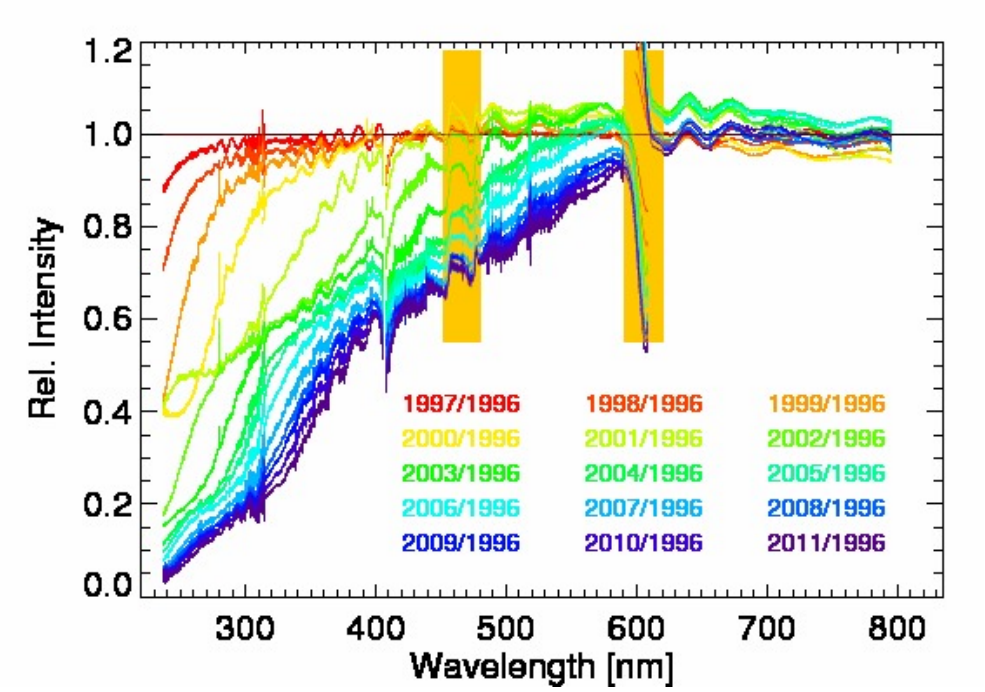

Figure 5-1 Degradation of instrument response: Solar spectra taken at the 3rd of July each year divided by the reference spectrum from 03-Jul-1996 (see text)

5.2 Level 0 to 1b Processing Concept

There are four basic calibration steps needed to convert the instrument binary data into calibrated physical quantities.

1. Signal processing: correction for dark signal, FPA crosstalk, pixel-to-pixel gain, and straylight
2. Wavelength calibration: assigning to each detector pixel its associated wavelength
3. Radiance calibration: conversion of the corrected detector signals of the earth-shine spectra to radiance units; this includes polarisation correction
4. Irradiance calibration: conversion of the corrected detector signals of the solar spectra to irradiance units; this includes correction for the BSDF of the diffuser plate.

Furthermore the measurements have to be geolocated, i.e. the geographical position of the footprint on the Earth's surface has to be determined from the instrument's scan mirror angle and from the spacecraft data.

In earlier GDP versions, all in-flight calibration constants were derived from the calibration measurements in the operational processing from level 0 to 1. The "Level 1 Product" contained the raw detector signals (binary ADC units) of the science measurements plus all necessary calibration constants (in modern terminology one would call this a Level 1a product). The end-user had to run an Extraction program which applies the calibration constants to the data; this inflates the Level 1 Product to a much larger "Level 1 data set" containing fully calibrated data (the difference is that the Product contains calibration data plus raw signals as 2-byte integers; the extracted data contain calibrated signals as 4-byte floats plus three 4-byte floats for wavelength, accuracy error and precision error). Apart from product size considerations, an additional advantage of this procedure was that the user could optionally omit certain calibrations to investigate their influence. On the downside, the proliferation of calibration options made the extraction process confusing.

In the current GDP version, a single L1b product with fully calibrated radiances and irradiances is generated, without showing intermediate calibration steps. This also implies that several algorithms from the previous algorithm description document have now vanished – because the calibration options provided by these algorithms were either considered too experimental, or were not used in operational Level 2 processing (in fact they still exist in software, but are not used anymore).

A high-level overview of the Processing Flow is given in Figure 5-2. In the next subsections we will give a more detailed description of the modules, but the concept is the following:

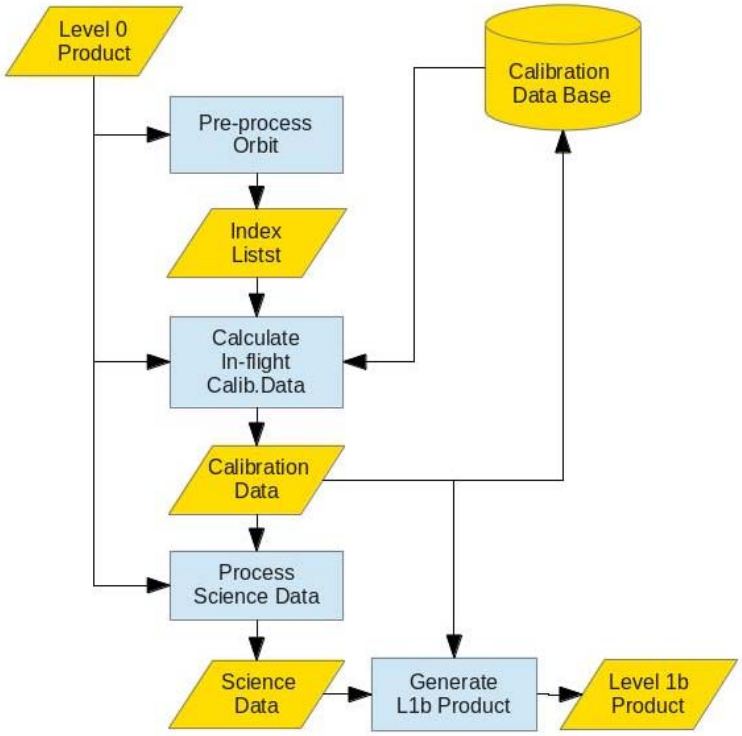

Figure 5-2 High-level data flow of Level 0-1b processing

- "Pre-process Orbit" makes a scan over the entire Level 0 product; lists are generated which link data packets to measurement type. Furthermore it is established which pre-disperser temperatures are encountered over the orbit – this is used to set up the data structures for temperature-dependent calibration data.
- "Calculate In-flight Calibration Data" uses the Level 0 data packets which have been indexed as calibration measurements to derive new in-flight calibration data. It updates the Calibration Database, and it retrieves from the Calibration Database all necessary calibration data which were not newly calculated.
- "Process Science Data" applies the calibration data obtained above to the radiance measurements (Earth, Moon) and the irradiance (Sun) measurements, and calculates the Level 1b radiances and irradiances (as well as geolocation).
- "Generate Level 1b Product" writes the radiances, irradiances, geolocation, and selected calibration parameters to the Level 1b product.

5.3 Overview of Level 0 to 1b processing flow

The high-level picture has been given above, see Figure 5-2. We will now discuss the processing steps more in detail and provide an overview of the Level 0 to 1b processing flow. Detailed algorithm descriptions are provided in Section 6.

5.3.1 Pre-process Orbit

This module browses the Level 0 product, and generates various lists:

- List with the measurement mode for each data packet (DP). The following modes are identified:
  DP_SCANNING (Earth radiance measurements, including nadir scanning, nadir "static" i.e. non-scanning, polar view scanning)
  DP_SUN (Solar irradiance measurements)
  DP_LAMP (Spectral Calibration lamp measurements for Spectral calibration)
  DP_LED (LED measurements for PPG calibration)
  DP_DARK (dark signal calibration measurements)
  DP_MOON (Moon measurements)
  DP_LAMP_DIFFUSER (calibration measurements of the spectral calibration lamp directed over the Sun diffuser)
  The various measurement modes are identified according to the position of the Scan Mirror (encoder readout). The list is set up as a data structure that may also hold additional measurement properties (see below)
- List of all Predisperser Prism temperatures which occur (in the DP_ lists above, the temperature of each measurement is given by a pointer to this list)
- List of all integration time patterns (set of ITs used for each channel) the which occur (in the DP_ lists above, the IT pattern of each measurement is given by a pointer to this list)
- List of all Scan Mirror angles which occur in this orbit; associated to each scan angle ω_{SM} is a list of predisper temperatures which occurred at than angle.
  The list is generated by the GetOmegaScanPosition routine; for every DP (1.5 s read-out) a weighted average is calculated for the 16 scan mirror positions in the DP, taking into account the acceleration and deceleration of the scan mirror and the scan direction (forward or backward)
- Geolocation list: sets up an (empty) geolocation data structure for each DP
- Polarisation list: set up an (empty) polarisation data structure for each DP

Further, the module does the following:

- identify calibration data packets in the SAA region, and delete these from the DP_DARK, DP_LED or DP_LAMP lists
- store orbit info (start/stop time, ERS-2 state vector) into the calibration database

5.3.2 Calculate In-flight Calibration Data

In this module, new calibration data are calculated from calibration measurements performed in the orbit. Furthermore, all calibration data that will be used for the science measurements are collected from the calibration database and, as far as applicable, interpolated to the temperature-dependent wavelength grids and the scan mirror angles that will be encountered in the processing (a list of these temperatures and scan angles has been prepared in preprocessing, see above).

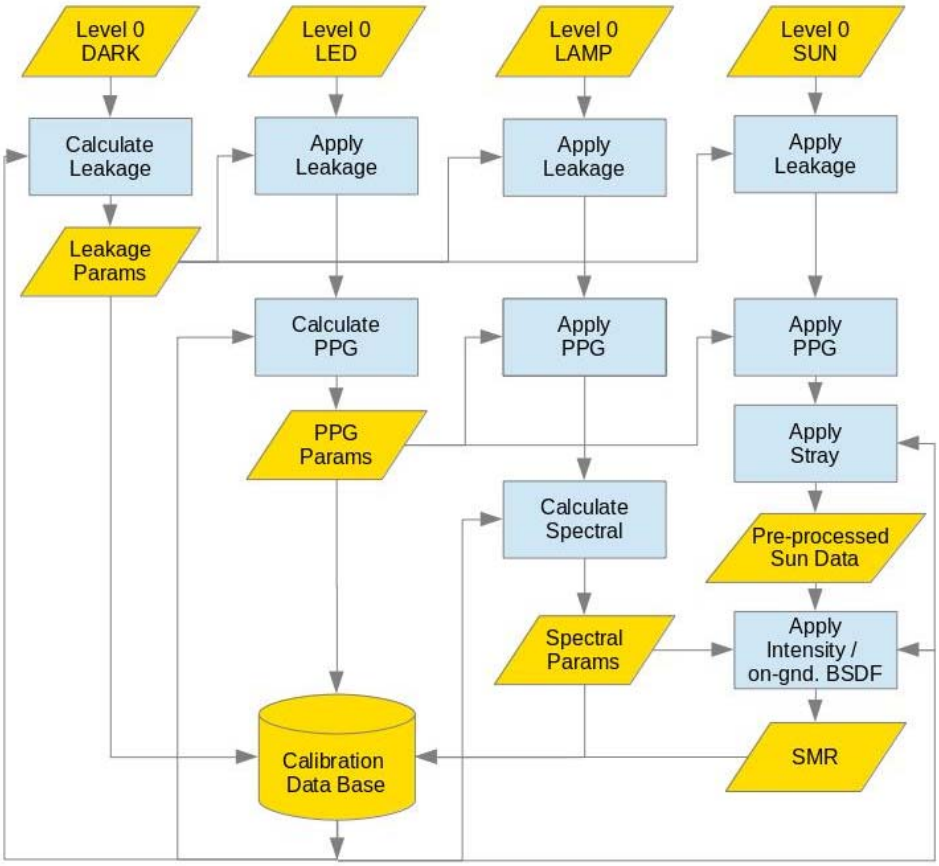

Figure 5-3 Processing flow for calculating calibration parameters from the measurements

The processing flow for calculating new calibration data is shown in Figure 5-3.

The following sequence of processing steps is performed (in this order):

- "Calculate Leakage": Process the measurements (data packets) from the DP_DARK list (see Section 5.3.1). For each integration time pattern, derive the dark signal of each channel pixel. Derive PMD offsets. Dark signal parameters for integration time patterns that are in the orbit list (from preprocessing), but for which no valid data are available, are fetched from the calibration database.
- "Calculate PPG": Process the measurements (data packets) from the DP_LED list and derive the Pixel-to-pixel gain (PPG) parameters. If no valid PPG data can be calculated, fetch these from the calibration database.
- "Calculate Spectral": Process the measurements (data packets) from the DP_LAMP list and derive the spectral coefficients, for the predisperser temperatures encountered in the orbit. If the list of predisperser temperatures from preprocessing contains temperatures that are not covered by in-flight measurements, fetch the corresponding spectral coefficients from the calibration database.

  Measurements from the DP_LAMP_DIFFUSER list are currently not used operationally
- "Calculate SMR": Process the measurements (data packets) from the DP_SUN list and derive the "Sun Mean Reference" spectrum (SMR). The Sun measurements are corrected for dark signal ("leakage"), for PPG, and for straylight. Then they are averaged into one spectrum. This is then corrected for the radiance response (from on-ground keydata), and for the BSDF from the on-ground keydata.
  For historical reasons, only the BSDF correction from on-ground is applied here, but not the better BSDF correction derived later in the mission from in-flight data (that will

be done in a later processing step). The reason for this was that, for a long time, instrument degradation and in-flight BSDF correction were simultaneously fitted on Sun measurements calibrated only with on-ground data.
The module also calculates the averaged Sun PMD measurements, and derives the PMD out-of-band factors, the “Q-factors”.

All newly calculated calibration parameters are stored in the calibration database.

After this is done, the calibration data for polarisation sensitivity and radiance sensitivity are collected from the database. These are then interpolated to all scan angle positions from the preprocessing list, and to all wavelength grids associated with the predisperser temperatures from the preprocessing list (this has an historic reason: in the older GDP versions that used an intermediate Level 1b product + extraction software, these calibration data had to be available to the extraction software which did not have database access – therefore all calibration data necessary to process the science measurements were collected and written to the Level 1b product).

5.3.3 Calculate Science Data

After the preprocessing and the calculation/assembly of calibration parameters, the science data are processed. An overview of the processing flow is shown in Figure 5-4.

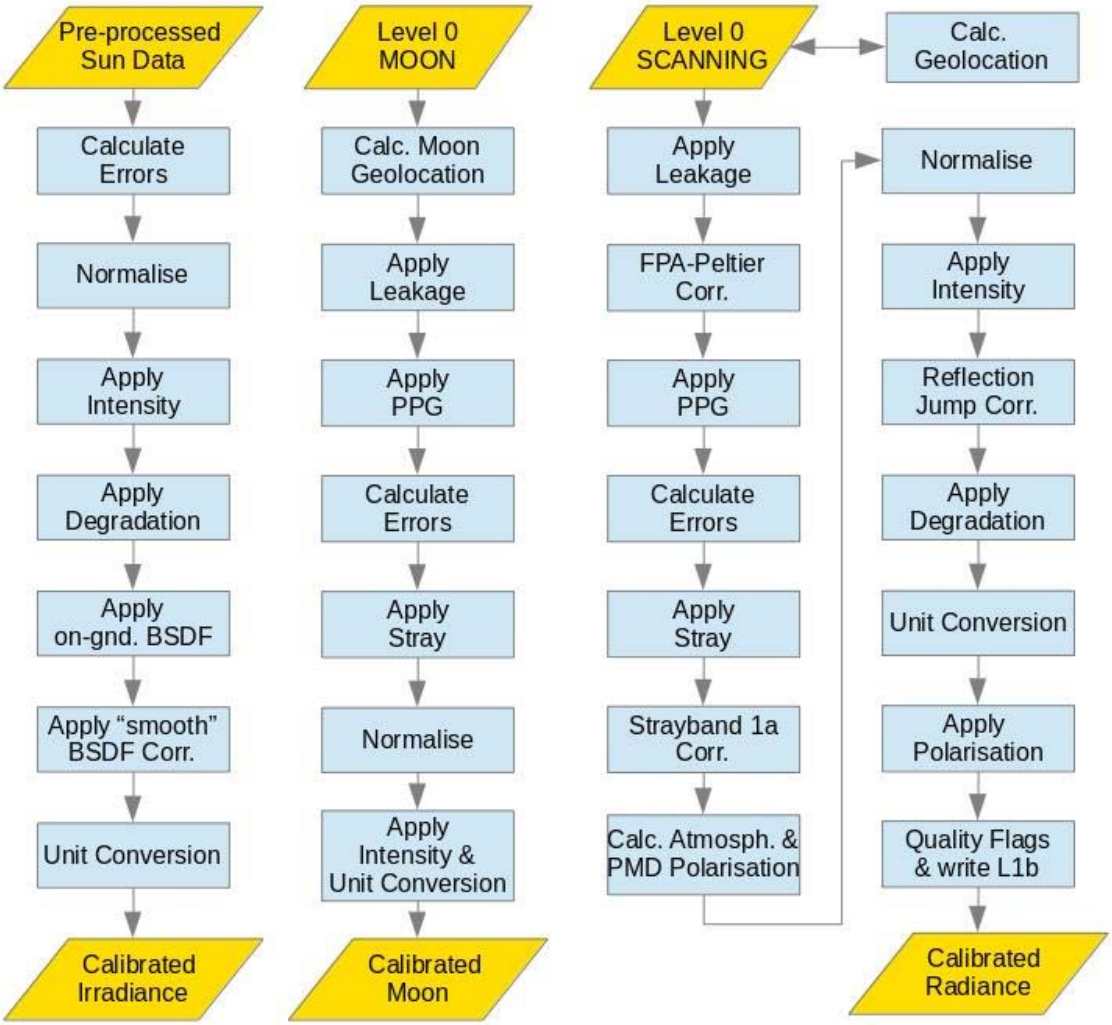

Figure 5-4 Processing flow for science measurements

As first step, the geolocation list that has been set up in preprocessing is filled. Then the data for each measurement mode (SUN, MOON, SCANNING) is processed. In the following, a short summary of algorithm steps is given, in the sequence of processing. For a detailed algorithm description, see Section 6.

GEOLOCATION:

In the geolocation processing, the instrument scan angle and time information is converted to geographical coordinates, and the solar illumination condition is determined. This relies heavily on the use of ESA's ERS-2 Orbit Propagator, whose routines will not be explained in detail here.

For each readout (by default every 1.5 seconds) geolocation parameters are calculated for start, middle, and end of the integration time. Note that, due to the sequential readout of the detectors, the real start/end of integration increases with pixel number. Geolocation corresponds to the first detector pixel in the readout. A separate geolocation is calculated for the PMDs, which are sampled 16 times per 1.5 seconds.

SUN:

As input for DP_SUN processing the Pre-processed Sun Data are used (see Figure 5-3), which are already corrected for Dark signal, PPG, and straylight. The processing flow is:

- Calculate errors
  derive the precision error for each measurement
- Normalise
  signal normalisation to 1 second exposure time
- Apply Intensity
  convert units from BU/s to "keydata units" Watts/(s.cm^3.sr) by dividing the signal by the Radiance Response function
- Apply Degradation
  divide the measured radiances by the instrument degradation function, to obtain radiances that are comparable to the Begin-of-Life state of the instrument
- Apply on-ground BSDF
  convert the measured radiances to Solar Irradiance in "keydata units" of Watts/(s.cm3), using the on-ground calibration of the Sun Diffuser's BSDF
- Apply 'smooth' BSDF correction
  remove residual seasonality effects from the BSDF function; the 'smooth' refers to the wavelength dependence which uses a polynomial
- Unit conversion
  convert from "keydata units" Watts/(s.cm^3) to photons/(s.cm^2.sr.nm)

MOON:

The processing flow for DP_MOON data packets is:

- Calculate Moon Geolocation
  another call to the Orbit Propagator is made for this specific mode
- Apply Leakage
  correct measurements for dark signal
- Apply PPG
  correct measurements for variations in Pixel-to-Pixel Gain
- Calculate errors
  derive the precision error for each measurement
- Apply Stray
  correct measurements for straylight

- Normalise
  signal normalisation to 1 second exposure time
- Apply Intensity
  convert units from BU/s to photons/(s.cm^2.sr.nm) by dividing the signal by the Radiance Response function and making the unit conversion (see above under SUN).

SCANNING:

The processing flow for DP_SCANNING data packets is:

- Apply Leakage
  correct measurements for dark signal
- FPA-Peltier correction
  correct signals with long integration time (band 1a) for cross-talk from the Peltier coolers of the FPA
- Apply PPG
  correct measurements for variations in Pixel-to-Pixel Gain
- Calculate errors
  derive the precision error for each measurement
- Apply Stray
  correct measurements for straylight
- Strayband 1a Correction
  uses the signal in the dedicated “straylight band” (a region at the beginning of the channel 1 detector) to perform an additional background correction (for e.g. uncorrected straylight, SAA-induced noise) on signals in Band 1a
- Init polarisation / calibrate PMDs
  calculate the “7 Fractional Polarisation Values”: single-scattering polarisation values and polarisation values derived from PMDs, and their effective wavelength
- Normalise
  signal normalisation to 1 second exposure time
- Apply Intensity
  convert units from BU/s to “keydata units” Watts/(s.cm^3.sr) by dividing the signal by the Radiance Response function
- Intensity Jump Correction
  rectify radiances for an intensity gradient during detector readout
- Apply Degradation
  divide the measured radiances by the instrument degradation function, to obtain radiances that are comparable to the Begin-of-Life state of the instrument
- Unit conversion
  convert radiances from “keydata units” to photons/(s.cm^2.sr.nm)
- Apply Polarisation
  The “7 Fractional Polarisation Values” are interpolated to wavelength. This is partly done using modified spline interpolation (Akima), partly using a parameterisation of the polarisation curve in the UV. From the interpolated polarisation values, a polarisation correction factor is derived for and applied to each channel array detector pixel
- Quality flags and product generation
  after the processing of scanning data is finished, the data product is generated and some data quality flags are written to the Level 1b product, e.g. for saturated pixels.

5.3.4 Update from the previous processor version

The “new” GOME L1b data product in NetCDF format (GDP Version 5.0) contains fully calibrated L1b data. This differs fundamentally from the “old” proprietary GOME Level 1 data format, which basically contained Level 1a data, and where a dedicated “extraction software” tool had to be applied to obtain the fully calibrated Level 1b data that are now in the “new” product.

The current L1b product corresponds to the following former extraction software command:

```
gdp01_ex -j -c "LAFSNIUP" –k –e <scdegrad> -f "yyyy" <scdegrad>
```

where:

-c “channel-options”:

L=Leakage,

A=FPA,

F=Fixed,

S=Straylight,

N=Normalize,

B=BSDF,

P=Polarisation (KNMI Polarisation),

I=Intensity,

U=Unit_Conversion

-j correct radiance jumps

-k switch off spectral cross-correlation (default is: on)

-e instrument degradation

-f smoothed BSDF correction (channel_filter = "CCCC" one "C" for each channel, where C='y' or C='n')

Former extraction options which are not applied are:

-a compute albedos instead of radiances

-u “unsmoothed BSDF” correction (channel_filter = "CCCC" one "C" for each channel, where C='y' or C='n')

-F reflectivity degradation correction (channel_filter = "CCCC" one "C" for each channel, where C='y' or C='n')

-G reflectivity degradation correction for O3 window (325 - 335nm) new mode

-P reflectivity degradation correction for PMD_1 new mode

The `<scdegrad>` file with “degradation” and other LUTs (now as version 5.00) is still input to the new processor.

6 Level 0 to 1 Algorithm description

6.1 Preamble

In this chapter, we describe the algorithms to be used in the GOME Level 0 to 1b processing. This concerns mainly the mathematical descriptions, including some backgrounds. The actual processing flow has been described in the previous section.

The algorithms described here relate to the building blocks shown in the processing flow diagrams, Figure 5-3 and Figure 5-4, although the sub-division into the various document chapters do not necessarily have a 1-to-1 correspondence to the building blocks.

General algorithm steps such as conversion to engineering units and calculation of the SAA exclusion zone for on-board calibration measurements are described in Sections 6.2 and 6.3.

Calculation of Dark signal corrections and related signal baseline corrections are described in Sections 6.4 to 6.6.

The correction for PPG, and the Straylight correction, can be found in Sections 6.7 and 6.8, respectively.

Spectral calibration is described in Section 6.9.

Radiometric calibration is in the GDP performed in a number of different processing steps. In the algorithm description, these are assembled in Section 6.10, with the exception of polarisation correction. Due to the extensive processing for the polarisation correction, this is described in a separate section (6.11).

The calculation of the radiance/irradiance precision errors and quality flags is described in Sections 6.12 and 6.13, respectively.

6.2 Conversion to Engineering Units

This “algorithm” is used in the pre-processing, when the level 0 product of the complete orbit is browsed to generate the various lists. In fact this is not a single algorithm module, but elements of this processing are used whenever a Level 0 data field needs to be interpreted.

The GOME data packages include a variety of data with different formats and meanings. Besides the detector array and PMD signals (which are expressed as binary units until the application of the radiometric calibration), there are the following categories of information:

digital information

these values are used as they appear; no further transformations are required. Example – frame counters.

enumerations

these data consist of either one bit or two bits which have a certain semantic meaning; no further transformations are required. Example – mode switches for detector array temperatures.

digitised analog measurements

these values are converted by the use of a polynomial (see below); e.g. temperatures of the optical bench.

time information

the time is given by a 32–bit wrap–around counter; the time correlation files received from MMCC are required to transform this counter into a UTC time (see below).

For the digitised analog information the following formula applies:

$$Y = a_3^* x^3 + a_2^* x^2 + a_1^* x + a_0^* \qquad \text{Eq.(6-1)}$$

where x denotes the digital input from the data package, Y the analog result value, and a* (i = 0..3) are the polynomial coefficients for a certain value of the data package.

The time correlation file is given at the ascending node of the corresponding orbit and consists of the following information:

- Orbit number;
- UTC_{days} (the number of days since the 1.1.1950);
- UTC_{msecs} (the milliseconds of the day);
- SBT_{TC} (the satellite binary counter of the above UTC time);
- SBT_{DP} (the satellite binary counter period which is the number of nanoseconds yielding one tick of the satellite binary counter)

The UTC time of the data package is calculated as follows:

$$UTC_{DP} = UTC_{TC} + \frac{SBT_{DP} - SBT_{TC}\, SBTP\ 10^{-6}}{86.400.00} \qquad \text{Eq.(6-2)}$$

where UTC_{DP} and UTC_{TC} are the UTC times in days of the data package and the time correlation file respectively. SBT_{DP} and SBT_{TC} are satellite binary counters of the data package and the time correlation file respectively. SBT_{DP} is the satellite binary counter period which is given in nanoseconds. The factor 10^{-6} is required to transform nanoseconds to milliseconds and 86.400.000 is the number of milliseconds in one day. UTC_{TC} is calculated as follows from the entries in the time correlation file:

$$UTC_{TC} = UTC_{days} + \frac{UTC_{msecs}}{86.400.00} \qquad \text{Eq.(6-3)}$$

Remark: The subtraction in Eq.(6-2) takes into account the wrap–around nature of the satellite binary time counter in the case when SBT_{DP} is close to zero and SBT_{TC} is close to $(2^{32}–1)$.

On the L1b data product, the orbit time is given in seconds relative to 01.01.1990. The time for each measurement (“delta_time”) is in seconds after midnight.

Note that each data package has time at the start of the integration time for the first detector pixel that is read out (pixel 1023).

6.3 Determine SAA region

It is known that in orbit regions affected by cosmic particle bombardments, in particular the South Atlantic Anomaly (SAA), the real background signal is higher than the usual dark signal. The measured spectra are also prone to intensity spikes caused by cosmic particles. This may affect especially the calibration measurements for dark signal and for PPG determination

For this reason, all calibration measurements in the SAA are discarded during preprocessing (see Section 5.3.1).

The algorithm to identify the SAA uses the signal from PMD 1. It has been found that the noise level on PMD 1 is a reliable indicator of the enhanced particle bombardment in the SAA region. The processing is as follows:

- group the PMD 1 measurements in *PMDnoisecheckwindow* data packets (default: 10 data packets, which have 16 PMD readouts each)
- for each group (default N=160 PMD readouts), determine the median.
  Calculate a noise value as:

$$PMD\_noise = \sqrt{\frac{1}{N}\sum_{n=1}^{N}(S_{PMD}(n) - median)^2}$$

- All calibration measurements corresponding to the group are considered in the SAA, if *PMD_noise* > *PMD_noise_threshold* (default value: 6).

PMDnoisecheckwindow and *PMD_noise_threshold* are parameters from the initialisation file.

6.4 Correction for Leakage Current and Determination of Noise

This section describes the algorithm for the “Calculate Leakage” and the “Apply Leakage” processing steps.

Introduction

The detectors used for the 4 channels of the GOME sensor are random access linear photo–diode arrays. One characteristic of these devices is a certain amount of leakage current. This is produced by thermal leakage and it is expected that this current will depend on the orbital position of the satellite and also the time into the mission (sensor degradation). Therefore it is necessary to continuously monitor the leakage current and associated noise, and this is done by means of periodically taken dark–side measurements. From these, one can correct the charge readouts of the detector pixels for any leakage current contribution.

The PMD detectors are non–integrating devices, and therefore do not have a leakage current. Nevertheless those detectors must be corrected for their zero offset and the noise level from dark–side measurements must be monitored.

For historical reasons, the processor uses the term “Leakage Correction”, although “Dark Signal Correction” would be more appropriate.

Algorithm

The following definitions are relevant:

$S_i^{measured,k}$	measured signal of detector pixel i with an integration time pattern k for complete detector arrays [BU]
S_i	signal of detector pixel i corrected for leakage current [BU]
I_i^{DC}	leakage current of detector pixel i [BU/s]
S_i^{FPN}	fixed pattern noise (electronic offset) of detector pixel i [BU]
t	integration time [s]
$S_i^{Dark,k}$	signal of detector pixel i taken under dark conditions with an integration time pattern k for complete detector arrays [BU]
$\overline{S_i^{Dark,k}}$	mean signal of detector pixel i with an integration time pattern k for complete detector arrays [BU]

In theory, the signal of a detector pixel consists of the following components:

$$S_i^{measured} = S_i + I_i^{DC} \cdot t + S_i^{FPN} \qquad \text{Eq.(6-4)}$$

However, due to a generation of cross–talk, when the different channels are not integrating with the same readout times, it is not possible to determine values of I_i^{DC} and S_i^{FPN} valid for all integration times. Instead, one must measure under dark conditions with the same integration time patterns as those employed for scanning and other calibration measurements. This requires at least 10 (the more the better) consecutive dark measurements for each integration time pattern; from these a mean value data-array of dark signals can be calculated:

$$\overline{S_i^{Dark,k}} = \frac{1}{n}\sum_{j=1}^{n}\left(S_i^{Dark,k}\right)_j \qquad \text{Eq.(6-5)}$$

This implies that the leakage current correction is simply the selection of the applicable mean dark signal data-array for integration time pattern k, and the subtraction of this array from the main measurement:

$$S_i = S_i^{measured,k} - \overline{S_i^{Dark,k}} \qquad \text{Eq.(6-6)}$$

Following the introduction of the co–adding mode for scanning measurements, the definition of an ”integration pattern” includes not only the integration time of each band and a flag indicating the integration completion, but also an additional flag indicating whether the co–adding mode was active or not. Measurements made using the co–adding mode may have a different leakage signal than measurements taken without co–adding.

> Note: Because of the low temperature (–38°C) of the detector arrays, the leakage current itself is very small (about 1 BU/s). Therefore, the change of the leakage current under illumination is so small that there is no need for a second correction, as was originally proposed in the literature [R4].

The noise on the signals of the detector pixel readouts is also expected to be very small and a constant over all detector pixels. All dark measurements (with the same integration time) from one orbit are used to calculate standard deviations for each detector pixel; the mean value of these standard deviations will yield the mean noise value for the detector pixel readouts.

For the PMDs, mean values of the dark measurements over the same orbit period are calculated to yield mean zero offsets. Mean noise values on the PMDs are calculated similarly to those of the detector arrays.

The following diagram (Figure 6-1) identifies the sequence of steps required for the correction of leakage current.

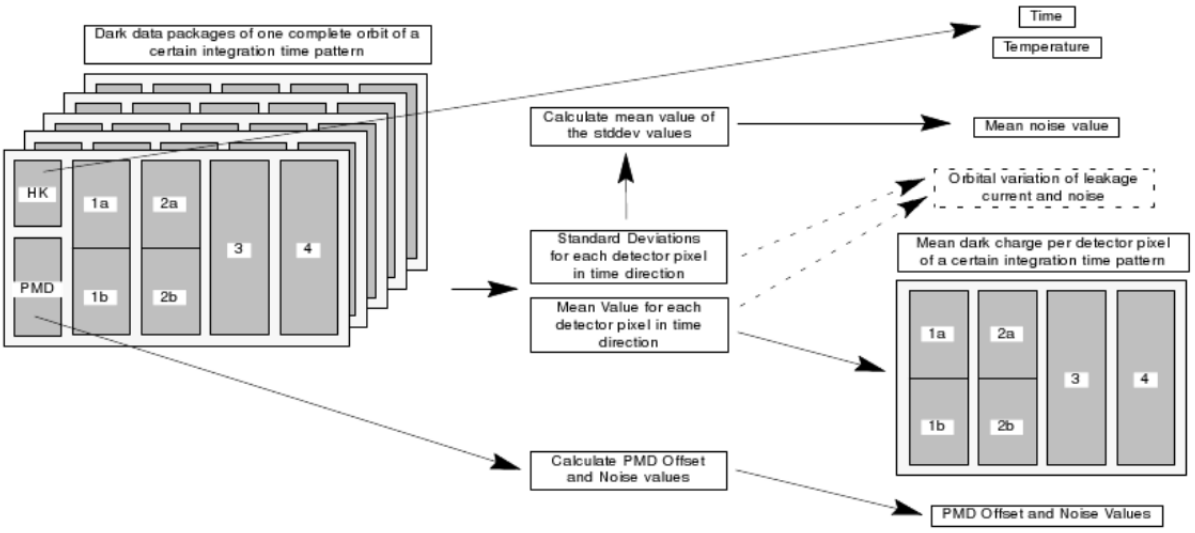

Figure 6-1 Correction for Leakage Current

Limitations

The fact that we only use one SAA boundary, although the background rises continuously towards the centre of the SAA, may cause some underestimation of dark signal in the region in or close to (but outside of) the SAA boundary. On the other hand, the dark signal might be slightly overestimated on orbits which directly follow an orbit where the SAA was measured at the night side, although most of this effect will be averaged out.

It is also known that, due to interference effects from the Peltier coolers, the real background signal may differ a little (plus or minus) from the calibrated one: this effect is addressed in the next section on FPA correction

6.5 Correction for FPA Noise

This Algorithm is based on the investigation of C. Caspar [R9]. An additional source of noise on the Reticon detector signal is correlated to the voltage controlling the Peltier coolers on the Focal Plane Assembly (FPA). The correction is only applied to Earthshine measurements.

This noise is correlated to the integration time. It can be determined by multiplying the Peltier cooler control signal by a scaling factor. This scaling factor is in fact dependent on the history of cooler switches, and thus should ideally be calculated anew for each orbit, using all measurements in that orbit. However, this conflicts with the GDP architectural requirement that each ground pixel shall be independently processable. Therefore, the scaling factor from one ‘typical’ orbit is used (has been added to the pre–flight calibration data) - the variation with orbit is expected to be ~10%. For each integration time, a different scaling factor is required. The magnitude of the effect scales with integration time; correction is only necessary for integration times of 6s or longer (band 1a measurements only).

The following steps are implemented in the correction for FPA noise :

- Collect all Peltier output signals of the orbit.
- Remove long–time trends in the Peltier output signals by applying a high pass filter:

  The software does this as convolution of the Peltier output signals from the whole orbit with a convolution kernel of 61 elements (from the keydata file). The first and last 30 measurements of the orbit, where the convolution delivers invalid results, are calculated using linear extrapolation. The first [last] and third [third last] convolved signals are used as basis for extrapolation.

  Subtracting the filtered (low pass) data from the Peltier output signals yields the high-pass filtered data.
- Calculate an average value of the Peltier outputs for the current integration period. Since Peltier signals are available every 1.5s, then for an integration period of 12s, a mean value of 8 Peltier outputs can be constructed.
- Calculate the FPA noise by multiplying the mean Peltier output by the (pre–flight) scaling factor specified for this integration time. Figure 3 shows typical FPA noise data for one orbit.
- Subtract the FPA noise from the signals of the entire band to be corrected

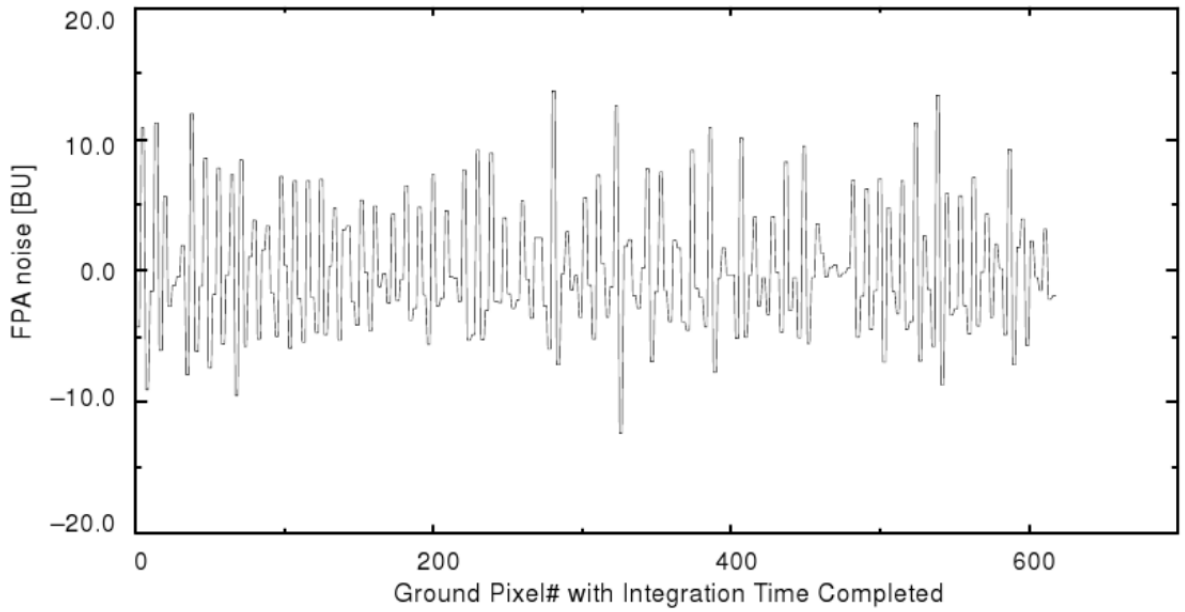

Figure 6-2 Typical FPA noise of one orbit

6.6 Apply Band 1a Residual Offset Correction

It appears that after removal of the Peltier crosstalk as described above, a residual offset remains which is too large for e.g. O3 profile retrieval (dark signal errors up to ±7 BU may remain for 12 seconds integration time; the typical uncertainty is ~3 BU). A correction of this residual offset, using the signal in the ”straylight 1a” band, is now implemented. The application of FPA correction is done in two steps: first the correction as described in Section 6.5, followed by straylight correction, and then correction for residual offset. Incidentally, the residual offset correction may also remove any enhanced background in the SAA that is not removed by dark current calibration.

This correction is based on the CHEOPS-GOME study of signal background [R15]. The results of this study are obtained by using a method where the correction is made after the correction for straylight.

> Note: one may argue that, from a point of principle, it might be better to apply this correction before the calculation of straylight, since straylight correction uses the amount of photons in the channel, which may be obtained from the signal corrected for dark signal and corrected for Peltier offset. Note, that this could only be implemented in an iterative approach, because the calculation of the amount of residual offset can only be done after straylight is removed. As the straylight correction is based on the total intensity in the channel, and as the number of counts in the Peltier correction is small compared to the total intensity, the error made in the straylight correction by not applying the residual offset correction first is expected to be negligible. Therefore, we stick to the procedure described in [R15] and implement this correction after the correction for straylight.

The offset is only corrected for long integration times, which limits it to channel 1a. Here we use the signal of the “straylight band 1a” just before the beginning of the nominal band 1a.

1. The algorithm uses the first 20 pixels of the straylight band 1a, starting at pixel 206 in channel 1 (we count from 0 in this description).
2. These are sorted w.r.t. signal intensity.
3. The intensity of the k-th sorted pixel is used to further correct the measurements.

We take k = 9 (i.e. the 10th sorted pixel when counting from 1).

The lower intensities not used because of noise, higher intensities are not used because they may be affected by cosmic rays or by straylight.

We then get for the signal S of pixel i in channel 1a:

$$S_{i\_1a}\,(\,corrected\,) = S_{i\_1a} - S_{k\_stray}\,(sorted) \qquad \text{Eq.(6-7)}$$

6.7 Correction for the Pixel–to–Pixel Gain

Introduction

One of the characteristics of a diode detector array is that the individual detector pixels have slightly different sensitivities. To correct for this feature, the determination of pixel–to–pixel gain (PPG) correction factors is required. Figure 6-3 shows typical PPG data (dotted line fine structure); the solid line is the smoothed PPG data (see below for explanation).

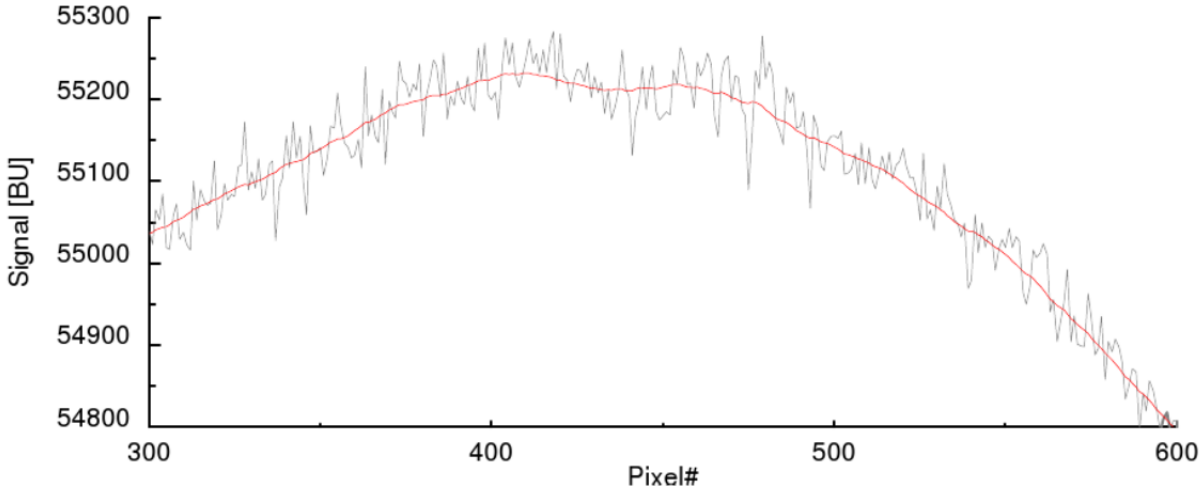

Figure 6-3 LED signal: example of “typical” Pixel-to-Pixel Gain data

Note: PPG is in principle contained in the instrument response function, but it is artificially separated from the instrument response function during calibration for the following reason:

- If the wavelength calibration of the instrument changes due to whatever mechanism, the radiometric response function of the instrument seen by a single detector pixel changes with it (this depends on wavelength-dependent transmission of lenses etc.).
- We have to re-interpolate the radiometric response to the wavelength of the detector pixel to be calibrated, but if pixel-to-pixel variations in quantum efficiency are present, the quantum efficiency of one pixel would be transferred to that of another pixel if the radiance response function were not corrected for PPG.
- The radiance response function in the GOME calibration Keydata is corrected for PPG, and so must be the detector signals before applying that function

From the GOME BBM calibration and characterisation at TPD, two results have emerged which are important for the PPG correction:

1. the variation of the sensitivity from one pixel to the other is around 0.2% (see figure 5). This means that the size of the absolute error is not very large. Nevertheless, when looking for weak absorption features the relative error (between individual pixels) could be of great importance.
2. Owing to reflections at lens mounting components of the BBM, the smooth illumination (3rd order polynomial) from the LED on the detector array was disturbed.

The conclusion from these observations was that the calculation and application of the PPG correction (leaving aside the coarse evaluation of defective or obstructed pixels) appeared to be unreasonable for this instrument, yet it was clear that an algorithm for PPG correction was required. The situation was improved considerably with the advent of constructive changes to the flight models (FM Several LED measurements corrected for dark current and FSM) to reduce these reflections. Now, instead of fitting a third order polynomial to the LED measurement as was initially proposed, a more sophisticated smoothing algorithm has been set up to assess the pixel–to–pixel gain correction factors.

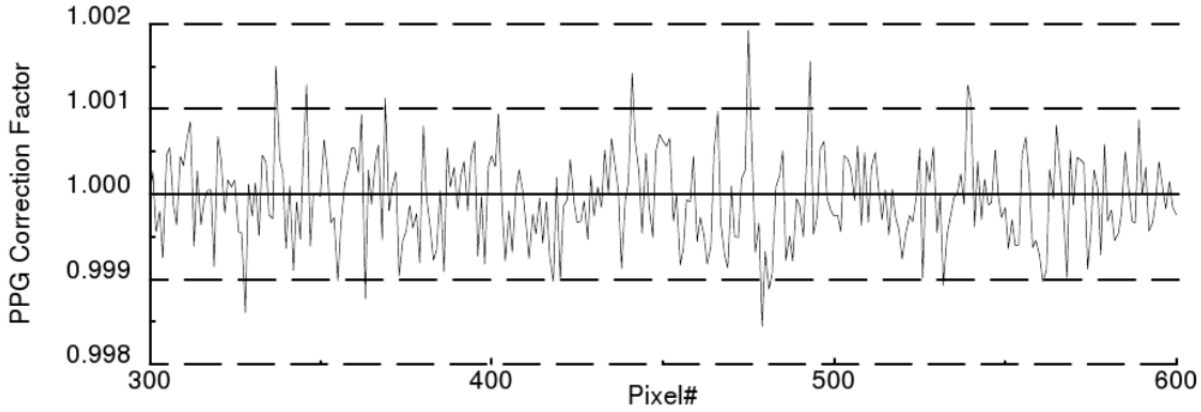

Figure 6-4 “Typical” Pixel-to-Pixel Gain Correction Factor (corresponding to Figure 6-3)

Algorithm

The following definitions are used:

S_i	measured scanning or sun calibration signal value of detector pixel i [BU]
S_i^{corr}	corrected scanning or sun calibration signal value of detector pixel i [BU]
S_i^{LED}	mean value of several measured LED signal values of detector pixel i [BU]
S_i^{smooth}	smoothed signal value of detector pixel i [BU]
c_i	pixel–to–pixel gain correction factor of detector pixel i [–]
n	smoothing value (width of triangle filtering window) [–]

The PPG correction factor is defined as follows:

$$c_i = \frac{S_i^{smooth}}{S_i^{LED}} \qquad \text{Eq.(6-8)}$$

where S_i^{LED} is the mean value of the signal values of several consecutive LED measurements and S_i^{smooth} the smoothed curve through this averaged measurements. The smoothed curve is calculated by means of:

$$S_i^{smooth} = \frac{\sum_{k=-n}^{n} \frac{n-|k|}{n} \cdot S_{i+k}^{LED}}{\sum_{k=-n}^{n} \frac{n-|k|}{n}} \qquad \text{Eq.(6-9)}$$

using a triangle filtering window of halfwidth n (default value: n=5). The application of the PPG correction is then simply:

$$S_i^{corr} = S_i \cdot c_i \qquad \text{Eq.(6-10)}$$

using the most recent PPG values from the calibration database. The PPG spectrum from the calibration database is updated in regular (baseline: monthly) intervals, following a LED calibration measurement

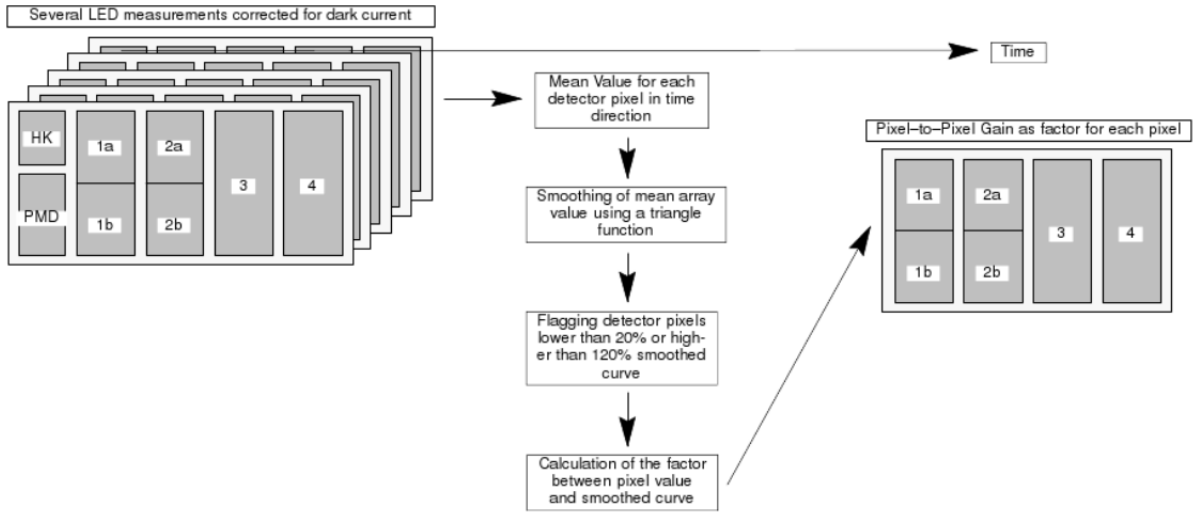

Figure 6-5 Correction for Pixel-to-Pixel Gain

6.8 Correction for Straylight

Introduction

After the first calibration and characterization measurements of the GOME BBM at TPD, it became obvious that straylight was a major issue; something which not only has to be characterized, but corrected for during the in–flight calibration exercise. Specifically in channel 1 and 2 the signal readouts are spoiled by a non–negligible amount of straylight. The following main sources of straylight in GOME were identified:

- a uniform (or very slowly changing) quantity of straylight over the detector pixels induced by diffuse reflections within the FPA;
- ghost straylight signals induced by reflections from the surfaces of the detector arrays and the lenses of the channel telescope. Two types of ghosts were detected during BBM calibration and characterisation (see [R3]):
    - symmetrical ghosts, which are signals mirrored at the middle of the detector array (close to pixel 512);
    - asymmetrical ghosts, which are signals mirrored at some arbitrary detector pixels.
- out–of–band straylight on the PMDs (induced by radiation outside the wavelength range of the array detectors).

The uniform straylight may be measured in the flight model (FM) by reserving specific detector pixel regions for straylight measurements (one region on the short wavelength end of the array detector spectrum area, the other on the long wavelength end). This has been done for channel 1 and 2. These detector pixels were not available for the BBM pre–flight calibration; they were assigned ’after the fact’. For channel 3 and 4, the short wavelength end of the detector arrays receive no signal higher than noise level. In addition, a relative level of uniform straylight w.r.t. the averaged signal level was determined during pre–flight FM calibration.

The ghost characteristics of the BBM have been evaluated thoroughly [G3]. The 3 characteristics of a ghost are (1) position of the center pixel in each channel about which

ghost signals are mirrored; (2) the efficiency (peak–to–peak ratio of ghost to parent) of the mirrored images; and (3) a ”focussing factor” (necessary because mirrored images are out of focus with the detector arrays, and parent images are not).

A number of modifications to the FM hardware and software were designed to reduce the unacceptable straylight levels noted in the BBM characterization. As a result, the straylight behavior of GOME FM and FSM has improved in several ways:

- asymmetric ghosts have disappeared (tilt changes to the gratings);
- Uniform and ghost straylight levels were reduced (use of anti–reflection coatings);
- relative straylight at the short wavelength side of channel 2 was reduced (change of the channel separation between channel 1 and 2);
- removal of important light leakage sources (improvement of internal baffling).

Despite these improvements, a correction algorithm for straylight is still required, at least for channels 1 and 2 of GOME FM and FSM.

PMDs:
A completely new discovery during the GOME FM calibration (see [G4]) was the detection of out–of–band straylight on the PMDs. All three PMDs receive light from above 800 nm, and one would expect this effect to be worst for PMD 1 (which has the lowest signal level in general). However, in orbit it was noticed that PMD 3 measured more signal than expected, while PMD 1 showed a negligible straylight effect. PMD 3 is especially sensitive to wavelengths above 790 nm, where the channel 4 spectral region ends. Because there are no means in GOME to measure light above 790 nm, the correction factor for the PMD signals would have to be estimated in some fashion from the expected spectral distribution of light collected by GOME in orbit. This is not constant, and so the straylight ratio for light above 790 nm is also not constant. However, the wavelength ranges beyond 790 nm for which the PMDs are sensitive were not calibrated on-ground.

Because of these unknowns, no straylight correction is done for the PMDs.

Instead the algorithm which calculates the fractional polarisation values for the PMD regions (see section 6.11.1) uses a correction factor (the “Q factor”) determined from Sun measurements. The Q factor is set to the value needed to obtain unpolarised irradiance (polarisation fracton = 0.5) from the Sun.

Algorithm

The straylight is calculated on a per channel basis. In the bands where at a certain readout not the whole channel is available, the straylight correction is only performed using the signals from the available datapoints: missing data are set to 0 (no attempt is made to estimate the intensity in the missing part of the channel). This can currently only happen for band 1b when band 1a is still integrating. It is not considered a problem since the total intensity in band 1a is small compared to that in band 1b.

The following steps are applied for the straylight correction of scanning and sun calibration data packets (after subtraction of leakage current and PPG corrections):

- normalisation of all signals by division with the integration time (yields signal fluxes);
- uniform straylight contributions
    - an averaged signal flux for all detector arrays is calculated;
    - the averaged signal fluxes per detector array are multiplied with the relative uniform straylight level values from pre–flight calibration (the uniform straylight levels are 0.2% for channels 1,2 and 0.1% for channels 3,4)
- ghost contributions

- mirroring of the measured signal flux around the pixel centers *s* for each ghost (*s* given per channel on the initialisation file; currently there is only one significant ghost);
- multiplication of the mirrored signal fluxes with the efficiencies *E* (initialisation parameter; 0.05% for channels 1,2,4 and 0.1% for channel 3) of the corresponding ghost. This is done as follows (pixels i are left of ghost center and pixels j are at right, factor 100 converts percentage to fraction):

  loop from *i*=*s*−1 to 0 and from *j*=*s*+1 to Ndet−1:

  $S\_ghost_i = S_j \cdot E/100$; $S\_ghost_j = S_i \cdot E/100$
- smoothing of S_ghost with the corresponding focusing factors (default: triangular smoothing kernel with halfwidth 3).

- array detector straylight correction
  - addition of the uniform and all ghost straylight contributions for each channel;
  - subtraction of the resulting absolute straylight flux multiplied by the integration time from the measured signal for each channel.
- multiply the corrected fluxes with the integration time

Accuracy:

The Calibration Keydata for straylight are probably not more accurate than ~10%; this uncertainty is not well characterised

The error on the signal due to errors in straylight subtraction manifests itself mainly as a precision error. This error is not explicitly included in the precision error calculation on the Level 1b data (see Section 6.12), however a lump-sump correction for several precision errors is taken into account

6.9 Spectral Calibration

Introduction

The objective of the spectral calibration is to assign a wavelength to each individual GOME detector pixel during the flight of the sensor. For this calibration, two steps are required:

1. *calculation* of the spectral calibration parameters from the calibration lamp measurements; this task again is separated into two steps:
   a. determination of the pixel number centre of the spectral lines and
   b. fitting of a polynomial through these pixel number/wavelength pairs;
2. *application* of these parameters to scanning and calibration data packets.

The wavelength calibration is expected to be sensitive to the dispersion of the pre-disperser prism, which may vary with temperature. Since indeed a correlation between spectral calibration and pre-disperser temperature has been found (also within an orbit), the spectral calibration parameters are stored in the calibration database as function of this temperature.

The polynomial coefficients in the calibration database are updated in regular (baseline: monthly) intervals, following a spectral line lamp calibration measurement. The Level 0 to 1b processing takes the most recent values from the database for the temperatures encountered in the orbit (see below).

Formulas

The following definitions are used:

S_i	signal of detector pixel i [BU/s]
N	sum of all signals which make up the spectral line [BU/s]
n_i	number of detector pixel i [–]
n_1 *or* n_2	certain numbers of a detector pixel [–]
$\bar{n}$	centroid of a spectral line as a fractional number of detector pixels [–]
λ_i	wavelength of detector pixel i [nm]
Var	variance of a spectral line as a fractional number of detector pixels [–]
σ	standard deviation of a spectral line as a fractional number of detector pixels [–]
$Skew$	skewness of a spectral line [–]
$FWHM$	full width half maximum of a spectral line as a fractional number of detector pixels [–]
a_i	coefficients of the spectral calibration polynomial for i = 0,...,4 [1/nm]

Figure 6-6 schematically shows a spectral line which might have been measured with GOME. One may regard such a data set as a statistical distribution, and use statistical methods to solve the pixel number positioning of the spectral lines, as discussed in [R2].

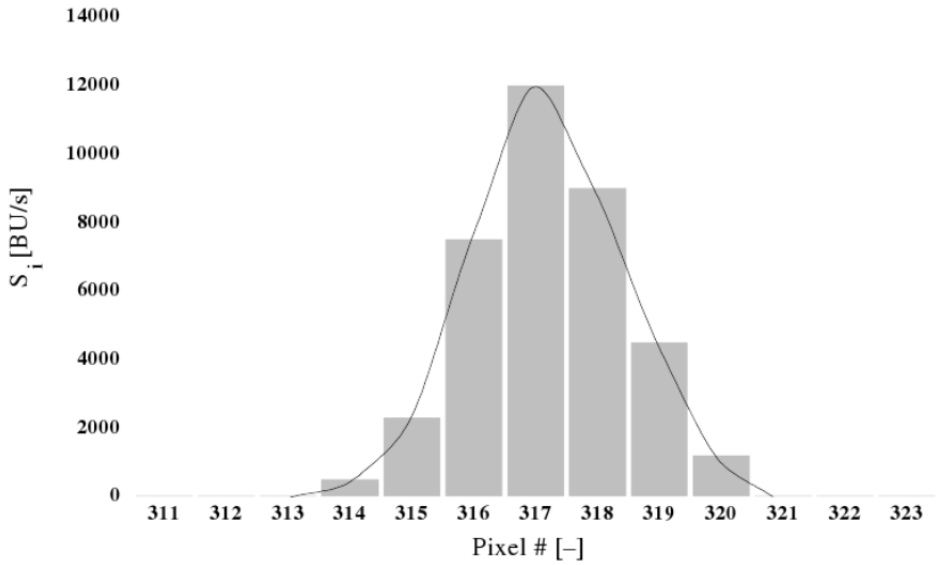

Figure 6-6 Schematic example of a spectral lamp line

In this application, the size N of the statistical sample is given by:

$$N = \sum_{i=n_1}^{n_2} S_i \qquad \text{Eq.(6-11)}$$

where S_i is the measured signal on detector pixel i and n_1 and n_2 are the first and last detector pixels which cover the spectral line.

One may then calculate the moments of the statistical signal distribution, which yield some characteristic information about the spectral line. These are:

1. the mean value

$$\overline{n} = \frac{1}{N} \cdot \sum_{i=n_1}^{n_2} i \cdot S_i \qquad \text{Eq.(6-12)}$$

2. the variance and standard deviation

$$Var = \frac{1}{N-1} \cdot \sum_{i=n_1}^{n_2} (i - \overline{n})^2 \cdot S_i \qquad \text{Eq.(6-13)}$$

$$\sigma = \sqrt{Var} \qquad \text{Eq.(6-14)}$$

3. the skewness

$$Skew = \frac{1}{N} \cdot \sum_{i=n_1}^{n_2} \left(\frac{i - \overline{n}}{\sigma}\right)^3 \cdot S_i \qquad \text{Eq.(6-15)}$$

For the positioning of spectral lines, the above statistical properties can be interpreted as follows:

1. The mean value gives the centroid of the spectral line, provided the other statistical properties fulfill certain prerequisites. The mean value is therefore the desired pixel centre result.
2. According to [R2], the full width half maximum (FWHM) of the line may be calculated as follows from the standard deviation σ :

$$FWHM = \sqrt{8 \cdot ln(2)} \cdot \sigma$$ Eq.(6-16)

3. While the mean and the standard deviation are dimensional quantities (that is, they have the same units as the measurement variables), the skewness (as defined here) is a non–dimensional number that characterises only the shape of the distribution, in our case the degree of asymmetry around the mean position of the spectral line. A positive (negative) value of skewness signifies a distribution with an asymmetry tail extending out towards more positive (negative) values. For Eq.(6-15) to be meaningful we need to have some idea of the standard deviation of this skewness statistic as an estimator of the skewness of the underlying distribution. For the idealised case of a normal distribution, the standard deviation of Eq.(6-14) is approximately $\sqrt{6/N}$. In practice, one should regard the skewness as significant only when it reaches values several times this number (see [R2]).

Once these statistics have been computed, one must then select lines (from a known pre–compiled list) for the fitting of a low–order polynomial. Selected lines should meet the following statistical criteria:

- the signal of the centre pixel shall not be below a certain minimum (well above the noise level);
- the FWHM shall not be below a certain value, in order to fulfill the Nyquist criteria for the digital recording of analogue signals;
- the skewness shall not be larger than a certain value (spectral lines are reasonably symmetric).

Extensive analysis of lamp spectra measured with GOME during the pre–flight measurements has been carried out to establish reasonable values for these criteria; the requirements should be as strict as possible, given that at least seven spectral lines per channel are needed for the polynomial fitting.

For each line, one has a mean pixel number and a known wavelength. For each channel, a polynomial is fitted to the line–selected pixel–number/wavelength pairs (using the Singular Value Decomposition Algorithm, as described in [R3]). The fitted coefficients a_k of this polynomial are the spectral calibration parameters for one detector array; these are given via

$$\lambda_i = \sum_{k=0}^{order} a_k \cdot i^k$$ Eq.(6-17)

where i is the pixel number (0..1023). The order of the wavelength polynomial is 3 for channels 1 and 2, and 4 for channels 3 and 4.

Algorithm

The following list (see also Figure 6-7) summarises the steps in level 0 to 1 spectral calibration algorithm; this is done per detector array.

1. Selection of lines that are defined in the pre–defined list of candidate lines for the spectral calibration (KeyData, initial pixel-wavelength list).
2. Search for spectral lines by shifting a window (9, 7, 5 and 3 detector pixel wide) over the detector pixel readings where the centre pixel has the highest reading and the surrounding pixels are decreasing to the outside of this window
3. Determination of the statistical moments as described in Eq.(6-12) - Eq.(6-16)
4. Selection of those lines which fulfil certain thresholds for the signal level of the centre pixel, the FWHM and the skewness; current values are:
   - $S\_centre\text{-}pixel \geq x$ BU/s with x =50 for channel 1 and x =300 for channels 2-4
   - $\sigma \geq 0.6$

- $FWHM \geq 1.5$
- $Skew \leq 0.6$

5. fitting of a polynomial through the selected pixel-number/wavelength pairs
6. store the coefficients in the database, together with the corresponding pre-disperser temperature.

The *application* of the spectral calibration is done as follows:

1. Find the most recent spectral polynomial coefficients that have the same pre-disperser temperature as the current one within a temperature limit of 0.1 K. If such coefficients cannot be found (this started to happen after the tape recorder failure in 2003) use the most recent coefficients within a temperature limit of 6 K.
2. Evaluate the polynomial for each detector pixel of each array.
3. [obsolete: apply a correction term based on cross-correlation – see below]

Line selection

To ensure a homogeneous data set, currently only those lines are selected in step 1 of the algorithm for calculating the coefficients, that satisfy the criteria from step 4, over the GOME lifetime, see [R23]. The corresponding line positions may be found on the processor's initialisation file.

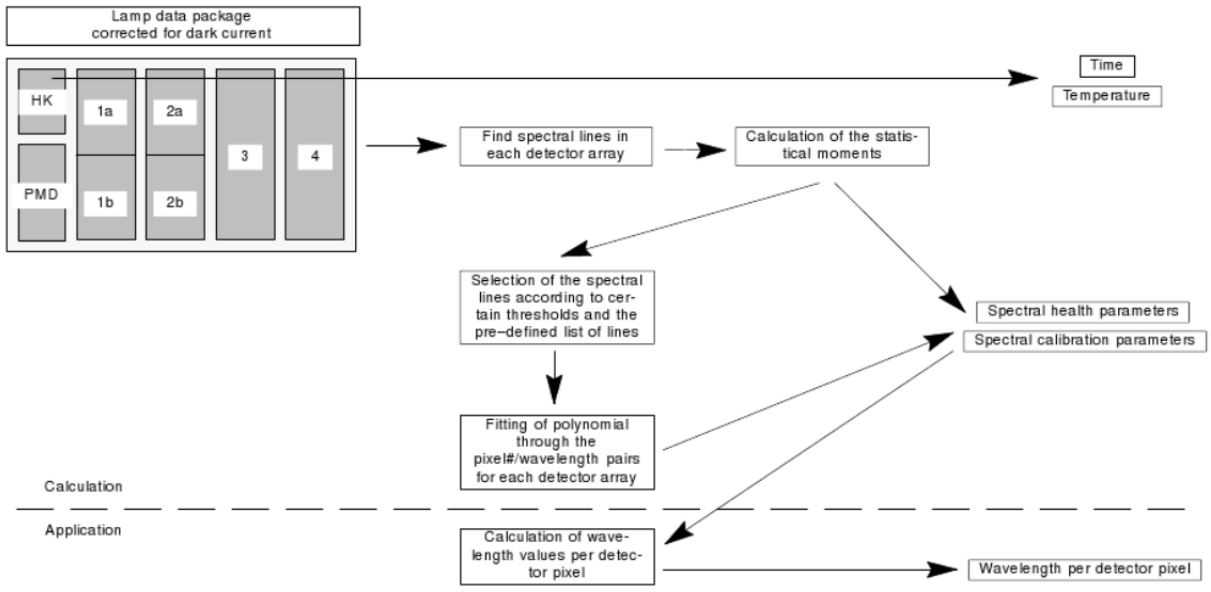

Figure 6-7 Spectral Calibration Algorithm

Obsolete: Correction of Spectral Calibration using Cross-correlation

In the previous GDP version (4.x) there was an option to add a correction polynomial, which was obtained from cross-correlation of a high-resolution theoretical solar spectrum and Sun measurements. In practice, this option was not used in the operational level 2 processing (or rather, level-2 processing did it itself). Therefore the option has been deleted for the current Level 1b product.

There also was a fixed correction polynomial, based on a cross-correlation made once by IFE, which was supposed to improve spectral calibration at the detector edges. Since it was not traceable what exactly had been done, in how far this correction should be time-

dependent, and since the cross-correlation now done in operational level 2 processing would overwrite that correction anyway, this also has been dropped from the processing in the current GDP version.

Accuracy

Wavelength calibration errors are typically 0.05 of a detector pixel. At the short wavelength side of channel 3 the error may be larger, due to the scarcity of lamp lines there.

As illustration, Figure 6-8 shows a lamp spectrum. Some 20 lines are visible here, though not all have been selected for fitting; while some of the non–showing lines (with low intensity for the scale of this plot) have been fitted. The plotted points represent the deviation (in pixel number, for each selected line) of the fitted wavelength, compared with the lamp line wavelength of the centroid. The deviation from the fitted wavelength (polynomial) is indicated by the right-hand scale of the figure.

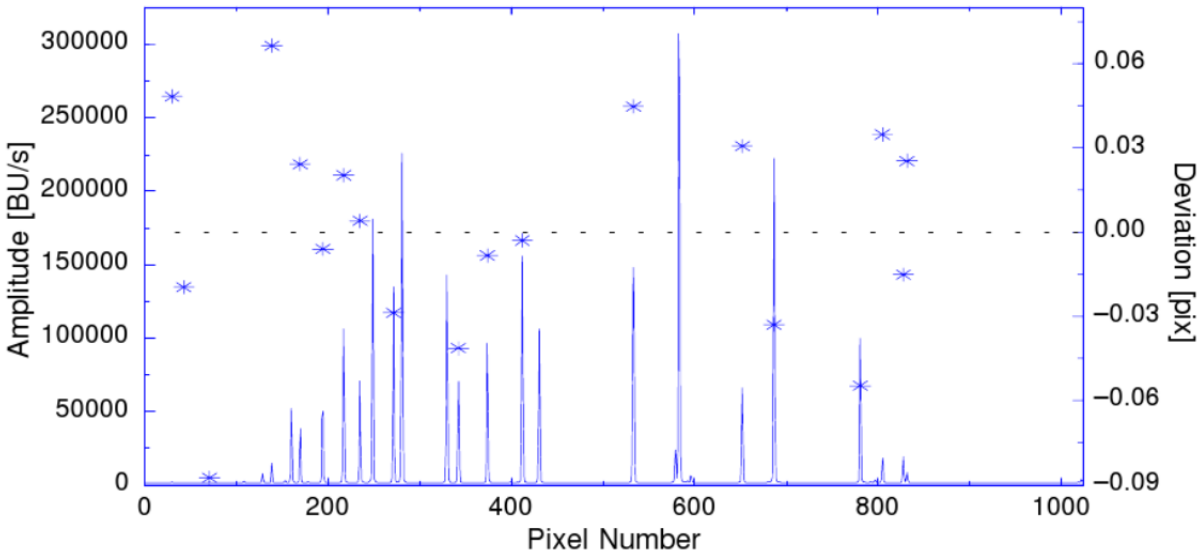

Figure 6-8 Example of Lamp measurement (solid line), selected positions (*) and their deviations of line centre w.r.t. fitted polynomial (right-hand scale)

6.10 Radiometric Calibration including degradation correction

This section gives a description of the intensity calibration using radiance response and diffuser BSDF calibration parameters. The polarisation correction algorithm (PCA) is described in the next section.

6.10.1 Introduction

The objective of the radiometric calibration is to transform the 16–bit binary units (BU) of the detector pixel readouts into calibrated radiances (photons s^{-1} cm^{-2} nm^{-1} sr^{-1}) or, for the Sun, calibrated irradiance (photons s^{-1} cm^{-2} nm^{-1}). The calibration is applied to three sources:

1. Sun: an intensity calibration using the GOME sun measurements taken via the diffuser in the calibration unit;
2. Earth: an intensity calibration including the application of a polarisation correction factor
3. Moon: a basic intensity calibration

The Moon calibration is treated like Earthshine (scanning) calibration, except that it does not take into account a (moon-phase dependent) polarisation correction. Note that Moon calibration also *does not* take into account the slit filling factor, which depends on the Moon's phase and the position of the GOME slit over the Lunar surface.

Figure 6-9 shows the schematic illumination configuration for the intensity calibration. During the sun calibration measurement the scan mirror of GOME is illuminated with sunlight via the diffuser and during the normal scanning operation the back–scattered light of the earth's atmosphere is entering GOME directly.

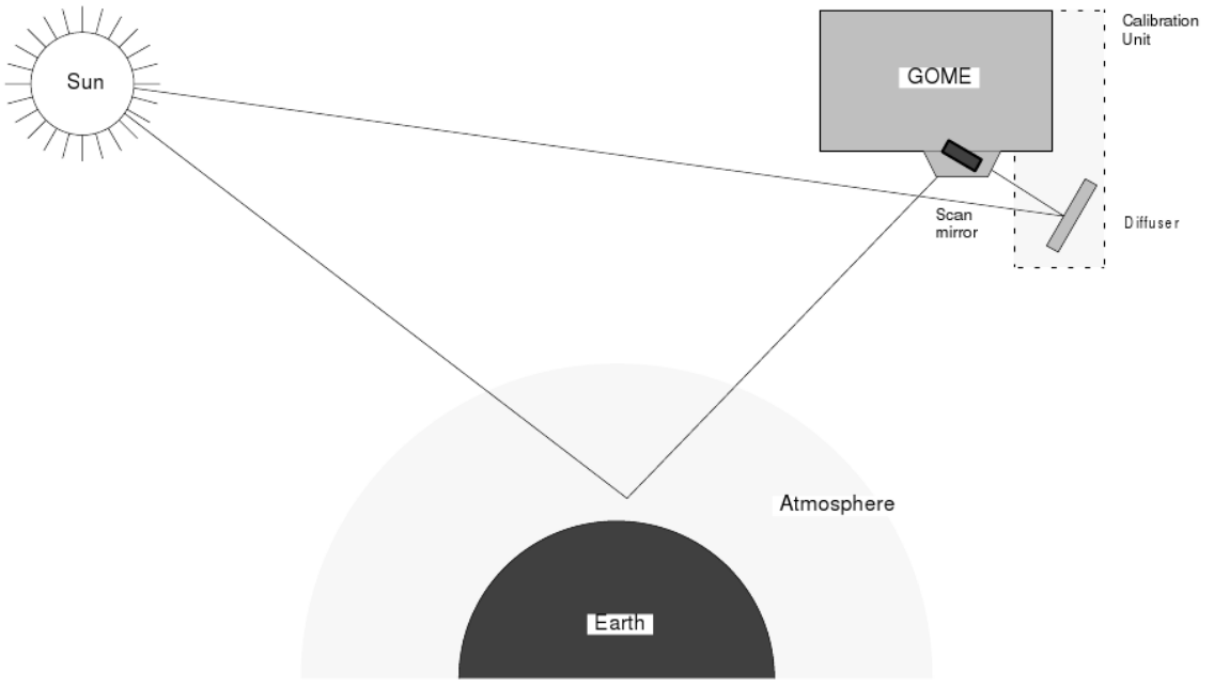

Figure 6-9 Schematic Illumination Configuration for the Intensity Calibration

In the processor, the radiometric calibration is divided in several steps. A basic calibration is carried out using the keydata from the on-ground calibration. Refinements are made to correct the radiance/irradiance for instrument degradation, and to correct the irradiance using an improved Azimuth dependence of the diffuser BSDF. The reason for this separation is

that historically, calibration using on-ground keydata was done inside the GDP Level 0-1b processing while degradation correction and improved diffuser azimuth correction was done by the GDP extraction software. The GDP extraction software also had an option to correct "radiance jumps" in Earth radiances. This is now added as standard processing step.

6.10.2 Calibration using on-ground keydata

Formulas

The following definitions are used:

$S_{i(readout)}$	signal of detector pixel i [BU/s] at module input (corrected for dark, PPG, straylight)
λ_i	wavelength [nm] of detector pixel i
t	integration time of a detector pixel [s]
S_i	time-normalised signal of detector pixel i [BU/s]
$S_{Sun,i}$	S_i from a Sun calibration measurement
$S_{Earth,i}$	S_i from a "scanning" measurement
$I_{Sun}(\lambda_i)$	irradiance transmitted from the Sun at wavelength λ_i [photons s^{-1} cm^{-2} nm^{-1}]
$I_{Earth}(\lambda_i)$	radiance back-scattered from the Earth at wavelength λ_i [photons s^{-1} cm^{-2} nm^{-1} sr^{-1}]
σ	scan mirror angle [degrees]
$H^*(\lambda_i, \sigma)$	radiance sensitivity function at wavelength λ_i and scan mirror angle σ [(BU s^{-1})/ (photons s^{-1} cm^{-2} nm^{-1} sr^{-1})]. The asterisk denotes that these correspond to keydata (quantities derived from the pre-flight calibration); however actual keydata use different units which are converted internally in the processor
$RR^*(\lambda_i)$	Radiance response function = $H^*(\lambda_i, \sigma)$ for nadir position and default temperature
$f_{SM}^*(\lambda_i, \sigma)$	Scan-angle dependent part of $H^*(\lambda_i, \sigma)$
$f2^*(\lambda_i, T)$	Temperature-dependent part of $H^*(\lambda_i, \sigma)$ for channel overlap region
$BSDF^*_{CU}(\lambda_i, Az, El)$	bi-directional scattering distribution function of the diffuser at wavelength λ_i and at specified azimuth and elevation angles [sr^{-1}]
Az	azimuth angle of Sun on diffuser (relative to central position)
El	elevation angle on of Sun diffuser (relative to central position)
c_pol_i	polarisation correction factor for the scanning measurements [–]

For each detector pixel, the signal readout (corrected for leakage current, pixel–to–pixel gain and straylight) is divided by the integration time to yield a normalised unit of binary units per second:

$$S_i = \frac{S_{i(readout)}}{t} \left[\frac{BU}{s}\right] \qquad \text{Eq.(6-18)}$$

For signals of a solar calibration measurement, the following calibration formula is valid (below the physical units of each term):

$$S_{Sun,i} = I_{Sun}(\lambda_i) \cdot H^*(\lambda_i, \sigma) \cdot BSDF^*_{CU}(\lambda_i, Az, El)$$
$$\left[\frac{\mathrm{BU}}{s}\right] = \left[\frac{\text{photons}}{\mathrm{s\ cm^2\ nm}}\right] \cdot \left[\frac{\mathrm{BU\ s^{-1}}}{\mathrm{photons\ s^{-1} cm^{-2} nm^{-1} sr^{-1}}}\right] \cdot [\mathrm{sr^{-1}}] \qquad \text{Eq.(6-19)}$$

where $S_{Sun,i}$ is the measured signal on the detector arrays, $I_{Sun}(\lambda_i)$ the irradiance transmitted from the Sun at the wavelength λ_i, $H^*(\lambda_i, \sigma)$ the radiance sensitivity function at the wavelength i and scan mirror angle σ, and $BSDF^*_{CU}(\lambda_i, Az, El)$ the bi-directional scattering

distribution function of the diffuser in the calibration unit, which is dependent on the wavelength, the azimuth and the elevation of the sunlight on the diffuser. For sun calibration measurements, σ will be taken as nadir, because the scan mirror dependence of the CU w.r.t. nadir is included in the keydata BSDF.

As mentioned in the introduction of this section, the calibration using keydata alone has some limitations, see also Eq.(5-4) for a more general description.

By inversion of the above formula, the irradiance of the sunlight is calculated as follows:

$$I_{Sun}(\lambda_i) = \frac{S_{Sun,i}}{H^*(\lambda_i,\sigma)\cdot BSDF^*_{CU}(\lambda_i, Az, El)} \qquad \text{Eq.(6-20)}$$

For the last factor (Sun signals divided by BSDF), also a mean value is computed from several sun observations; this value is the 'Sun Mean Reference' (SMR). This SMR is then divided by the radiance response factor $H^*(\lambda_i, \sigma)$.

In this processing step, the BSDF from on-ground calibration keydata is used. For individual Sun measurements, but not for the SMR, a further in-flight correction will be applied (see Section 6.10.4). The reason for not applying the in-flight correction to the SMR, is that this correction has been derived with SMR data as input.

The BSDF is expressed as parametrisation using polynomials, with coefficients *c* coming from the keydata file:

$$BSDF^*_{CU}(\lambda_i, Az, El) = (1 + c^*_{El}\cdot El)\cdot\left(1 - c^*_{Az}\cdot Az^2\right)\cdot\left(1 + \sum_{k=1}^{7} c^*_k \cdot (\lambda - \lambda_0)^k\right) \qquad \text{Eq.(6-21)}$$

where the azimuth angle Az is calculated as the solar azimuth angle at satellite minus an offset (from the initialisation file);
λ_0 is an offset wavelength (500 nm) to make numerical values smaller.

The radiance response is also a compound function, calculated from wavelength-dependent parts and a scan angle dependent part; in addition there is an "f2" function which corrects for the fact that the channel overlaps shift somewhat with temperature:

$$H^*(\lambda_i,\sigma) = RR^*(\lambda_i)\cdot f^*_{SM}(\lambda_i,\sigma)\cdot f2^*(\lambda_i, T) \qquad \text{Eq.(6-22)}$$

where the keydata $f^*_{SM}(\lambda_i,\sigma)$ and $f2^*(\lambda_i, T)$ are given per channel, for 9 scan angles and for 5 tempeatures, respectively. These keydata are interpolated to the actual scan angle and temperature of the mesasurement.

There will be 30 seconds of Sun calibration measurements during one orbit out of the 14 orbits per day. To ensure that the Sun is completely in the field of view of the diffuser, there are limits set on azimuth and elevation angle for the measurements to be used in the computation of the SMR.

Note that the wavelength calibration used here is based on the spectral lamp measurements which are derived in the GOME rest frame. The Sunlight itself will be Doppler-shifted as GOME moves towards the Sun under an angle of 21.5° + Az .

The application of radiance response for scanning measurements is likewise given by:

$$I_{Earth}(\lambda_i) = \frac{S_{Earth,i}}{H^*(\lambda_i,\sigma)} \qquad \text{Eq.(6-23)}$$

So far, we have assumed that $I_{Earth}(\lambda_i)$ and the signal at the entrance slit of GOME are unpolarised. However, the atmosphere polarises the incident solar light. Thus, a polarisation correction factor c_pol_i will be multiplied to the intensity of the scanning measurements. This factor will be described in the next section. In the processor, the application of the polarisation correction is done in a separate processing module independent from the application of radiance response.

6.10.3 Correct degradation of the radiance response

In all GOME wavelength regions there is degradation caused by hard UV light and cosmic radiation. Pixel-dependent degradation, caused by cosmic radiation, will be accounted for by changes in the PPG calibration. We here describe corrections to the smooth part of the instrument response. An introduction has already been provided in Section 5.1.5.

The following definitions are used:

λ	wavelength [nm]
t	elapsed time since start of GOME measurements
t_0	reference day for degradation (default: 03-JUL-1995 12:01:21)
$I_{Sun}(\lambda,t)$	irradiance transmitted from the sun dependent on time and wavelength
$I_{SunCorr}(\lambda,t_{meas})$	irradiance at measurement time, corrected for degradation
$P_{Deg}(\lambda,t)$	degradation function dependent on time and wavelength
$C_{SED}(t)$	Sun–Earth distance intensity correction
$Residual(\lambda,t)$	remaining structure of degradation algorithm
$a_k(t)$	polynomial degradation parameters for solar spectra $I_{SUN}(\lambda,t)$
LUT	look-up table for time dependent series of $a_k(t)$

The following algorithm for degradation correction, based on solar measurements, was developed by DLR in the framework of the ESA/ESRIN–project GDAQI. The principle approach is to monitor the changes, using ratios of all solar spectra with a measurement of a reference day (t_0) in the early GOME lifetime, as given in Eq.(6-24). This is explained in detail in [R11],[R18]. The dominant part of the degradation influence can be found by study of the solar irradiance of the Mean Sun Measurements, because most of the light path via the critical optical parts is identical for all measuring modes. For the Earthshine measurements, an additional scan angle dependence is present. However, due to the atmopspheric variability this is not straightforward to determine and could only be done using statistical methods. In the current Level 0-1b processing the scan angle effect is neglected.

The ratio of a solar spectrum at time t, relative to the spectrum at reference date t_0, may be written as

$$\frac{I_{Sun}(\lambda,t)}{I_{Sun}(\lambda,t_0)} = P_{Deg}(\lambda,t)\cdot C_{SED}(t)\cdot Residual(\lambda,t) \qquad \text{Eq.(6-24)}$$

where $P_{Deg}(\lambda,t)$ is the used degradation function dependent on time and wavelength, $C_{SED}(t)$ is the intensity correction due to the seasonal variation in Sun-Earth distance, and *Residual*(λ,t) is the remaining structure.

As noted in Section 5.1.5, a variable broadband Etalon structure is present in all detector channels, together with a change of the dichroic structures for the detector channels 3 and 4. These effects are not taken into account and are found as remaining structures in the residuals.

A two–step approach has been chosen to describe the degradation function P_{Deg} (λ ,t):

- Each irradiance ratio is approximated by a polynomial function in wavelength
- Each coefficient $a_k(t)$ of this polynomial in wavelength is described by a time dependent expression (in [R11] a polynomial fit in time, now a filtered time series)

Thus, for the degradation function $P_{Deg}(\lambda, t)$ following expressions have been obtained:

$$P_{Deg}(\lambda, t) = \sum_{k=0}^{n} a_k(t) \cdot (\lambda - \lambda_0)^k \qquad \text{Eq.(6-25)}$$

Each coefficient $a_k(t)$ of this polynomial in wavelength is taken from a LUT, with the coefficient listed as function of time. The LUT is generated by smoothing the time series of each polynomial wavelength coefficient (derived from polynomial wavelength fit of each solar spectrum ratio) with a Savitzky-Golay filter [R3]. Currently the filter width used is 250 days.

As mentioned in Section 5.1.5, the generation of the LUT is done outside the Level 0 to 1b processing. Inside the processor, we just apply the calibration constants for degradation:

$$I_{SunCorr}(\lambda_i, t_{meas}) = I_{Sun}(\lambda_i, t_{meas}) \,/\, P_{Deg}(\lambda, t_{meas}) \qquad \text{Eq.(6-26)}$$

where t_{meas} is the time of measurement, and $P_{Deg}(\lambda, t_{meas})$ is the degradation function, calculated from coefficients $a_k(t_{meas})$ that have been interpolated from the times associated to the LUT entries to t_{meas}.

6.10.4 Solar irradiance: Correct seasonal variation in BSDF

This correction is based on the CHEOPS-GOME study of seasonal variability of the diffuser BSDF [R14] (see also [W3]). The BSDF is described as polynomial function of solar azimuth angle on the diffuser.

Two approaches are presented in the study:

- using a smoothed BSDF which is a 3rd order polynomial fit in wavelength; this is provided for all channels
- a spectrally resolved BSDF, which can be provided for channels 1,3,4 but not for channel 2; this is because the frequent changes in etalon structure in channel 2 destroys the information in the analysis [R14]. As it may be that the spectral structure correlates with the detector etalon (although this is not obvious from the data) there may also be a real limitation for channel 2 here.

The CHEOPS-GOME study mentions that the spectrally resolved (or 'unsmoothed') BSDF should be used with care, especially in channels 3 and 4. In these channels there is a strong dependence of high-frequency structures (probably from interference in the dichroic filter) on solar azimuth angle on the diffuser. Especially after the problems with the ERS-2 gyros after 2001, this angle as given on the Level 1 product has some uncertainties. Furthermore, the features are only defined w.r.t. Azimuth angle 0, not in an absolute radiometric sense. For this reason we have chosen not to implement the spectrally resolved BSDF, but to use the smoothed BSDF correction.

The CHEOPS-GOME study on diffuser BSDF [R14] proposes to fit the azimuth dependence with a polynomial. However, the data volume concerned is not a problem for the GDP extraction software. We can obtain a higher accuracy by using a look-up table (LUT) for a number of azimuth angles.

For the smoothed BSDF, the wavelength dependence for each azimuth angle is calculated as an Nth (default: 3rd) order polynomial; the coefficients of this polynomial are in the LUT with dimensions (M, N+1) where the number of rows, M, is the number of azimuth angles.

For an azimuth angle $\alpha_{azi}(m)$, the smoothed BSDF as function of measurement wavelength λ_i for each pixel i is given by:

$$BSDF(\lambda_i, \alpha_{azi}(m)) = \sum_{j=0}^{N} LUT_{mj} \cdot (\lambda_i - \lambda_c)^j \qquad \text{Eq.(6-27)}$$

where λ_c is a 'central wavelength' in the channel (to keep the numerical values of LUT_{mj} in a smaller range of magnitude).

For an azimuth angle α_{azi}(m) ≤ Az ≤ α_{azi}(m + 1) , the BSDF is calculated for table indices (m) and (m+1) and then linearly interpolated to Az.

Note that the above correction is only applied to individual Sun measurements, not to the SMR.

6.10.5 Earthshine radiance: Correction of "Radiance Jump" effect

The detector arrays of GOME were designed for serial readout, such that the last pixel of the array is read out 0.09375 seconds later than the first. When GOME is scanning over an inhomogeneous ground scene (e.g. broken clouds) the variation of upwelling radiance with time is reflected in a variation of intensity depending on read-out time; the ground-scene inhomogeneity is aliased in the spectrum (this effect is denoted as 'spatial aliasing'). Such aliasing is often visible as a jump in radiance between two detectors (e.g. the last pixels of channel 3 record the same wavelengths as the first pixels in channel 4, but at an integration time which is shifted by ~0.09 seconds - although they should record the same intensity over a homogeneous scene there may be a radiance 'jump' if intensity varies with time).

Using information from the PMDs, which are read out every 0.09375 seconds synchronised with detector pixel 1, a correction can be applied to re-normalise all spectral intensities to the intensity measured at the integration time of pixel 1 of the arrays - this is also the time for which the geolocation is defined (note: pixel number 1024 is read 93.75 ms *before* pixel 1).

The algorithm has been described in detail in [R8].

Note that this correction only adjusts the absolute radiance levels; it cannot correct for the spectral changes in absorption line depth or Ring effect with changing ground scene. Also, it can correct only a linear trend.

6.11 Polarisation Correction

GOME is a polarisation sensitive instrument. The radiance response function described in the previous section calibrates the instrument assuming unpolarised input light. Therefore, a correction factor must be applied which describes the ratio

c_pol =

(instrument throughput for the actual input polarisation) / (throughput for unpolarised light).

This correction needs the polarisation sensitivity of the instrument and a characterisation of the atmospheric polarisation.

The polarisation correction algorithm (PCA) is divided into two main parts:

1. derive the atmospheric polarisation from theory and from measurement; this can only be done for a few wavelengths (this is processing step “calc. atmosph. & PMD polarisation” in Figure 5-4)
2. interpolate the polarisation points to wavelength and apply the polarisation correction to the spectrum (this is processing step “apply polarisation” in Figure 5-4)

6.11.1 Atmospheric polarisation from measurements

The atmospheric polarisation may be retrieved from the measurements, whenever we have two simultaneous measurements with different sensitivity to polarisation.

For the GOME spectral range, there are six wavelength regions which are covered by two detectors having different polarisation sensitivities – these are (see schematic Figure 6-10):

(a) the three Polarisation Measurement Devices (PMDs) which overlap the wavelength ranges of channels 2, 3 and 4, and

(b) the three overlapping regions of the channels themselves.

The first task of the Polarisation Correction Algorithm (PCA) is to calculate 6 values of fractional polarisation for the 3 overlapping and 3 PMD wavelength regions. A seventh point on the polarisation curve is supplied from a model calculation. The numbering of these points is illustrated in Figure 6-12 “Wavelength interpolation of the polarisation points”. As mentioned in Section 4, under “Channel separator”, the channel overlap points (at λ_4, λ_5, λ_6) are no longer being used in the wavelength interpolation, as their reliability was judged to be too low. In the current GDP version, polarisation from overlaps is also no longer calculated, although the original numbering has been maintained for historic reasons.

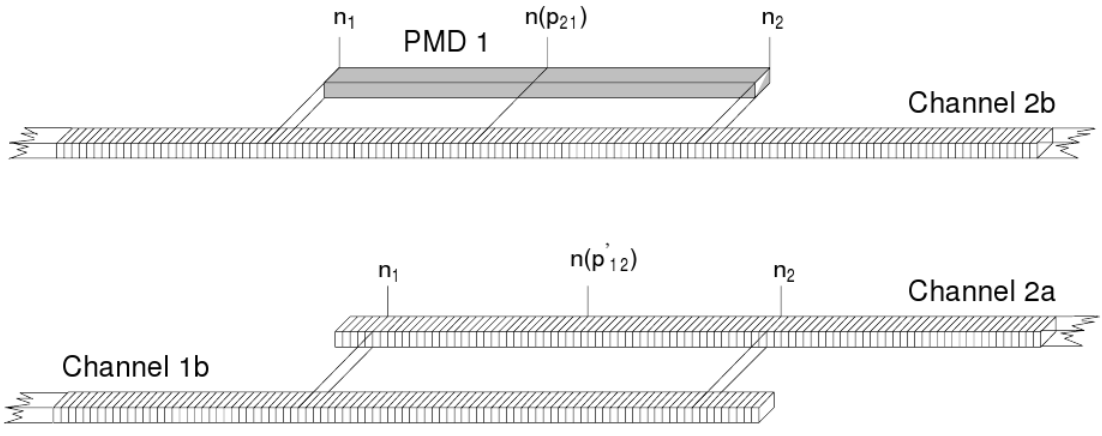

Figure 6-10 Configuration of the polarisation sensitive Detector overlaps (schematic)

For the overlap of PMDs with channels, the polarisation is calculated as following.

The measured signal of a channel detector pixel i may be written as:

$$S_i = a_{p,i} \cdot I_{p,i} + a_{s,i} \cdot I_{s,i} = a_{p,i} \cdot p_i \cdot I_i + a_{s,i} \cdot (1 - p_i) \cdot I_i \quad \text{Eq.(6-28)}$$

where S_i is the measured signal, p_i the fractional polarisation (the fraction of light polarised parallel to the slit), and $a_{p,i}$ and $a_{s,i}$ are the wavelength-dependent polarisation sensitivities of the corresponding polarisation directions (p=parallel, s=perpendicular); I_i is the total intensity, $I_{p,i}$ and $I_{s,i}$ are the intensities of the parallel and perpendicular polarised light entering GOME.

For the PMD detectors, the measured signal is given by:

$$S_{PMD} = d_{p,PMD} \cdot I_{p,PMD} = d_{p,PMD} \cdot p \cdot I_{PMD} \quad \text{Eq.(6-29)}$$

where S_{PMD} is the measured signal of a certain PMD and $d_{p,PMD}$ is the parallel polarisation sensitivity of the PMD. It is a design feature of the instrument that the perpendicular sensitivity of the PMDs is practically zero.

By comparing the signal measured by the PMD (from p-polarised intensity) with the signal measured by the array detector pixels, which is a mixture of s- and p-polarised intensities, it is possible to derive the polarisation fraction p. A problem in this comparison is that the PMD bandwidth is much larger (factor ≥ 1000) than the array detector's pixel bandwidth.

To solve this, we think of the PMD detector as a 'virtual array detector' with 'virtual pixels' which have exactly the same spectral bandwidth as the pixels of the corresponding channel array detector. We can then write the PMD signal (or intensity) as the sum over all virtual pixels of the spectral signal (intensity):

$$S_{PMD} = \sum_i d_{p,i} \cdot I_{p,i} = \sum_i d_{p,i} \cdot p_i \cdot I_i \quad \text{Eq.(6-30)}$$

To retrieve the atmospheric polarisation, further information needed is the ratio η of s- to p-polarised sensitivity of the channels, and also the ratio ξ of PMD-to-channel sensitivity for monochromatic p-polarised input. These have been measured during on-ground calibration:

$$\eta_i = \frac{a_{s.i}}{a_{p,i}} \quad \text{Eq.(6-31)}$$

$$\xi_i^* = \frac{d_{p.i}}{a_{p,i}} \quad \text{Eq.(6-32)}$$

The ratio ξ is independent of scan angle, but η is not. In the on-ground calibration data η is split into a function for the nadir position and a scan angle correction:

$$\eta_i = \eta_{nadir,i}^* \cdot \chi^*(\lambda_i, \Omega) \quad \text{Eq.(6-33)}$$

where $\chi^*(\lambda_i,\Omega)$ is the correction factor for the scan mirror angle Ω at the wavelength λ_i (the asterisk denotes calibration keydata).

The above expressions are in fact only valid if there is no mixing between the parallel and perpendicular polarisation components within the instrument. GOME has been designed to achieve this, by having the optical axes of all optical components in one plane. However, in the similarly designed SCIAMACHY instrument, it was found that polarisation mixing does occur. The probable cause being an optical retarding effect in the pre-disperser prism. In retrospect, also the GOME on-ground calibration data show tell-tale signs of such an effect (in particular discontinuities of the scan angle dependence at channel boundaries), albeit smaller. Since no calibration measurements were carried out that could quantify this effect, there is little we can do, and it will be assumed that Eq.(6-28) to Eq.(6-33) are valid.

Definition of the polarisation coordinate frame

The PMDs measure intensity polarised parallel to the spectrometer's slit. If we define the plane of polarisation to be coincident with the local meridian plane (through viewing direction and through nadir; this coincides with the scanning plane), see Figure 6-11, then the PMDs measures the $-Q$ Stokes Intensity.

In the GOME calibration algorithm, the polarisation is described using the fraction of light polarised parallel to the spectrometer's slit. This polarisation parameter is denoted p and is a simple transformation of the Stokes fraction Q/I given by:

$$p = 0.5 \cdot (1 - Q/I) \qquad \text{Eq.(6-34)}$$

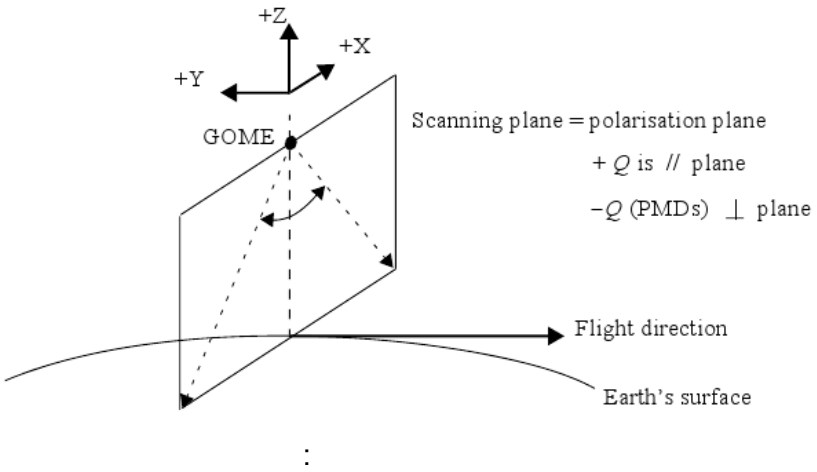

Figure 6-11: Definition of the polarisation plane for PMDs

Formulas

The following definitions are (have been) used in the text (the asterisk denotes calibration keydata):

λ_i	wavelength [nm] of detector pixel i ; whenever a detector pixel is mentioned in the following text, it is assumed that the wavelength corresponding to the pixel is known for the current set of wavelength calibration parameters
I	total intensity of the incoming light [W m^{-2} nm^{-1} sr^{-1}]
$I_{p,i}$ / $I_{s,i}$	intensity of the parallel / perpendicular polarised light at wavelength λ_i [W m^{-2} nm^{-1} sr^{-1}]
I_{PMD}	total intensity of the light reaching a PMD [W m^{-2} nm^{-1} sr^{-1}]
$I_{p,PMD}$	intensity of the parallel polarised light reaching a PMD [W m^{-2} nm^{-1} sr^{-1}]
p	(band-averaged) fractional polarisation value [–]
p_i	fractional polarisation value at wavelength λ_i [–]
$n(p)$	weighted mean pixel number of a certain fractional polarisation value [–]
S_i	signal of detector pixel i [BU] at input of this module
$S_{p,i}$ / $S_{s,i}$	signal of detector pixel i taken during a measurement for a completely polarised beam in the parallel (p) / perpendicular (s) direction [BU]
$a_{p,i}$ / $a_{s,i}$	parallel / perpendicular polarisation sensitivity of detector pixel i [–]
S_{PMD}	signal of a PMD, integrated over the exposure time of the corresponding array

	channel [BU]
$d_{p,PMD}$	parallel polarisation sensitivity of a PMD [–]
$d_{p.i}$	parallel polarisation sensitivity of a ”virtual” PMD pixel [–]
$\eta^*_{nadir,i}$	polarisation sensitivity ratio of detector pixel i [–]; these (keydata) values are given for the nadir position of the scan mirror
η_i	polarisation sensitivity ratio of detector pixel i [–]; it is assumed that the appropriate scan mirror angle correction factor has been applied
ξ^*_i	polarisation sensitivity ratio of PMD ”virtual” pixel i to array detector pixel i [–]; these values are given for each PMD
Ω	scan mirror angle [degrees]
$\chi^*(\lambda_i,\Omega)$	polarisation sensitivity correction factor for wavelength λ_i and scan mirror angle position Ω [–]

Polarisation from PMDs

The following description concentrates on the evaluation of one fractional polarisation value for a given PMD region, for example with PMD 1 and the corresponding channel regions. The other PMDs are treated similarly.

Using formula Eq.(6-28) we may write the pixel intensity as follows:

$$I_i = \frac{S_i}{a_{p,i} \cdot p + a_{s,i} \cdot (1-p)}$$

We now assume that *p is a constant* for a given PMD wavelength range. Substituting the above in Eq.(6-30) we obtain the “PMD virtual pixel sum”:

$$S_{PMD} = \sum_i d_{p,i} \cdot p \cdot \frac{S_i}{a_{p,i} \cdot p + a_{s,i} \cdot (1-p)}$$

$$S_{PMD} = \sum_i \xi_i^* \cdot p \cdot \frac{S_i}{\eta_i + p(1-\eta_i)} \qquad \text{Eq.(6-35)}$$

using the definitions of ξ and η from Eq.(6-31) and Eq.(6-32) respectively [in the formula above it is implicitly assumed that η is corrected for the nadir–viewing scan mirror angle position Ω].

Eq.(6-35) is the basic expression for deriving the p value; a numerical solution must be applied. In the Level 0-to-1b processor this is done using the ZBRENT algorithm [R3].

There are three such equations (for the 3 PMDs). Care must be taken to include all detector pixel signals for which ξ^*_i is non–zero; this implies using channel data over more than one band. Further, the PMD signals must be integrated over the same exposure time as the corresponding bands.

A corresponding result can be written for the solar measurements T_{PMD} and T_i. Since it is known that solar extra-terrestrial light is unpolarised (p=1/2), we have:

$$T_{PMD} = \sum_i \xi_i^* \cdot \frac{T_i}{\eta_i^{SUN} + 1} \qquad \text{Eq.(6-36)}$$

where η_i^{SUN} denotes the polarisation sensitivity corrected for the solar position of the scan mirror.

There are no unknowns here, so assuming no PMD straylight or out-of-band light (light beyond the spectral range covered by the PMDs), Eq.(6-35) for solar measurements should be identically true. The difference between the two sides of this equation is then a measure of the PMD straylight / out-of-band light, for an unpolarised light source.

We may define a relative correction factor for these Sun measurements :

$$Q_{SUN} = \frac{(T_{PMD} - T_{VS})}{T_{PMD}} \qquad \text{Eq.(6-37)}$$

where T_{VS} is the virtual sum on the right hand side of Eq.(6-35).

The virtual sum for the earthshine measurements Eq.(6-35) can be similarly re-cast with a straylight correction term:

$$S_{PMD} = \sum_i \xi_i^* \cdot p \cdot \frac{S_i}{\eta_i + p(1-\eta_i)} + Q_{EARTH} \cdot S_{PMD} \qquad \text{Eq.(6-38)}$$

Unfortunately Q_{EARTH} cannot be equated to the (known) solar straylight correction Q_{SUN} , because the polarisation state of the atmosphere in the straylight region is not known. However, assuming the polarisation for a given PMD takes the same (constant) value in the straylight region, we may use the following rough estimate:

$$Q_{EARTH} = 2 \cdot p \cdot \frac{T_{PMD}}{S_{PMD}} \cdot Q_{SUN} \qquad \text{Eq.(6-39)}$$

where for T_{PMD} we use the PMD value from the Sun Mean Reference
(note that the PMD values on the Level 1b product for the scanning measurements are Sun-normalised and are thus giving S_{PMD}/T_{PMD} for each PMD readout).

Note that in practice the Q factors for Earth and Sun do not only correct straylight and/or out-of-band light, but in fact also provide a rough self-calibration on the Sun in case of errors on keydata, including the effects of instrument degradation on the polarisation sensitivities. If the degradation takes place in the common light path of PMDs and channels, i.e. before the PMD split-off, the effect of instrument degradation on ξ^*_i may be small. Since it is believed that most of the degradation occurs in the scan mirror, this may indeed be the case (with the exception of the spectral regions which show changes in the response of the Dichroic). However, η and its dependence on scan angle Ω may change in the case of scan mirror degradation.

Wavelength of fractional polarisation values

Here we assign a representative wavelength for the single p–value assumed constant over the PMD wavelength range. Rather than placing this point at the middle of the range, it is situated at some pixel center of gravity found by weighting the array detector signals over this range. The formula applied for this weighting is:

$$n(p) = int\left(\sum_{j=0}^{4095} S_j \cdot \xi_j^* \cdot j \Big/ \sum_{j=0}^{4095} S_j \cdot \xi_j^*\right) \qquad \text{Eq.(6-40)}$$

where S_j is the signal of each individual pixel, and ξ_j the polarisation sensitivity of each individual pixel.

Since the PMDs may extend over more than one channel, and all four GOME channels together have a grand total of 4096 detector pixels, the loop is extended to cover this number of indices.

6.11.2 Atmospheric polarisation from theory

For the UV part of the spectrum a fractional polarisation value may be derived from a model calculation. Below ~300 nm, polarisation is dominated by Rayleigh scattering, and a simple calculation based on a Rayleigh single–scattering model (see [R5]) will return a constant value depending only on the illumination geometry. This is a useful adjunct to the p–values derived from GOME measurements, since the last available measurement point is the first overlap (around 312.5 nm) – the wavelength region 300–325 nm contains the strongest variation of atmospheric polarisation, and any additional pointers to the polarisation in this region are useful.

The *degree of polarisation P* (not pol. fraction *p*) due to single scattering by molecules is

$$P_{ss} = \frac{1 - cos^2\Theta}{1 + \Delta + cos^2\Theta} \qquad \text{Eq.(6-41)}$$

where Δ is an anisotropy constant related to the Rayleigh depolarisation ratio (Δ = 0.0574 for depolarisation ratio 0.0295), and Θ is the scattering angle at a representative scatter height in the atmosphere (~30 km for wavelengths less than 300 nm). Θ is given by :

$$cos\Theta = -cos\,\theta\ cos\,\theta_o + sin\,\theta\ sin\,\theta_0\, cos(\Phi - \Phi_0) \qquad \text{Eq.(6-42)}$$

where θ, θ_0 and φ – φ_0 are the *local geometrical angles* at the *scattering height*: line–of–sight zenith, solar zenith and relative azimuth respectively. Note that these angles must be derived from the geolocation information – the conversion from satellite height to scatter height and the derivation of local angles follows standard results from spherical trigonometry.

Also required is the angle of the polarisation plane (with respect to the local meridian plane). This is given by:

$$\chi_{ss} = \begin{cases} 180 - \beta\ (if\ \sin\beta\ \geq 0) \\ -\beta\ (if\ \sin\beta\ < 0) \end{cases} \qquad \text{Eq.(6-43)}$$

$$\sin\beta = \frac{\cos\theta_0 + \cos\theta\cos\theta}{\sin\theta\sin\Theta}$$

When θ = 0, the local meridian plane is not defined (direct nadir view), and χ_{ss} is then taken as the angle between the scanning plane and the perpendicular to the plane of incident sunlight. For more details of this special case, see [R5].

The relation between degree of polarisation P and fractional polarisation p_7 is given by:

$$1 - p_7 = \frac{1 + P_{ss}\cos 2\,\chi_{ss}}{2} \qquad \text{Eq.(6-44)}$$

We follow here the convention used in the calibration of GOME (p = fractional polarisation parallel to GOME optics); the original seventh point formulation in [R5] specified p for the perpendicular optics direction – hence the (1–p) in Eq.(6-44).

Although the degree of polarisation Pss has greater physical meaning, it is more convenient in the calculation of the polarisation correction factor (see section 6.11.2) to use the fractional polarisation p. Model studies have shown that equation Eq.(6-41) for Pss is valid for λ less than 300 nm, while the plane of polarisation angle χ remains very close to χ_{ss} over the whole GOME range.

Once the geolocation is known, p_7 can be calculated readily. Orbit simulations show that the value of p follows the solar zenith curve quite closely, and there are some variations across the swath (east versus west pixels) – this is especially true for the large swath width option (960 km).

To obtain a representative value of p_7 over the 960 km swath width, the following is done:

- for each 1.5 second readout, a value Q_I = $P_{ss}\cos 2\,\chi_{ss}$ is calculated for angles at the start, middle, and end of the integration time. An average of Q_I is build using a weighted mean:

$$Q\_I\_mean = (0.5 \cdot Q\_I_{start} + Q\_I_{mid} + 0.5 \cdot Q\_I_{end})/2 \qquad \text{Eq.(6-45)}$$

- The representative value of $P_{ss}\cos 2\,\chi_{ss}$ to use in Eq.(6-44) is taken as the average of Q_I_mean over all 1.5 second readouts within the exposure time.

Wavelength of the 7th point

The interpolation of polarisation in wavelength (see Section 6.11.3) will need the limit λ_{SS} below which the polarisation from Rayleigh single scattering may be used. The connection to the polarisation points derived from the PMDs will also need a "wavelength of steepest gradient" λ_m. In the most simple implementation, λ_{SS} is fixed at 300 nm and λ_m is derived based on a connection point to the PMD values.

An improved algorithm has been proposed by Schutgens and Stammes [R20]. Here, λ_{SS} and λ_m are parameterised as function of airmass, ground albedo and ozone content:

$$\lambda_{SS} = a_0 + \sum_{i=1}^{2} a_i / M^i + b_i \cdot \left(\frac{VCD}{VCD_0} - 1\right) \qquad \text{Eq.(6-46)}$$

$$\lambda_m = \sum_{i=0}^{2}\sum_{j=1}^{2} c_{ij} / M^i \cdot A^j + \sum_{i=1}^{2} d_i \cdot \left(\frac{VCD}{VCD_0} - 1\right)^i \qquad \text{Eq.(6-47)}$$

where *M* is the airmass, A is the surface albedo, and *VCD* is the vertical ozone column [DU]; VCD_0 = 345.8 DU.

The parameters have been fitted from model calculations as:

$$a = [308.68 \quad -29.10 \quad -29.10]$$

$$b = [0.0 \quad 7.58 \quad -4.26]$$

$$c = \begin{bmatrix} 316.43 & -41.89 & 29.49 \\ 0.33 & -0.06 & 0.66 \\ -1.11 & 0.56 & -3.46 \end{bmatrix}$$

$$d = [0.0 \quad 7.20 \quad -4.08]$$

where for c_{ij} index i runs over column and index j over row

In the GomeCal algorithm from KNMI [R21], this parameterisation has been implemented using the Fortuyn-Kelder ozone climatology [R22] to calculate VCD, whereas the albedo is calculated by comparing the measured GOME reflectance at 380 nm with a pre-calculated lookup table. We have followed this implementation of albedo here. The calculation goes as follows:

- the 3-dimensional LUT from KNMI is mapped to a 4-dimensional LUT [reflectance, cos(SZA), relative azimuth, pixeltype]. There are 18 entries for reflectance in the range 0 to 1.0, 10 for SZA in the range 5 – 85°, 5 relative azimuths, and 8 pixel types. For the pixel type, indices 0-3 correspond to the GOME pixel types 0-3 for the 960 km swath ("East", "Nadir", "West", backscan)., indices 4-7 correspond to the GOME pixel types for swaths where the difference in line-of sight (LOS) angle between the start and the end of the integration time is <8°; if this LOS difference is <4 then nadir static is assumed with pixeltype=5; and if the LOS difference for a backscan pixel is <25° then pixeltype=7.

- the reflectance is calculated by applying a triangular weighting function over 11 pixels around 380 nm of the ratio radiance / irradiance. To this end, the SMR is interpolated in wavelength to the wavelength grid of the scanning measurement before the ratio is build. Note that degradation correction is not necessary here, since the processing assumes that degradation is independent of scan angle and in that case is divides out in the ratio radiance/irradiance.
- the values of the LUT are, for the given pixel type, linearly interpolated to the relative azimuth, cos(SZA) and reflectivity of the measurement (in that order). This yields the albedo at 380 nm.

In GDP version 4, we also used the Fortuyn-Kelder ozone climatology. The current Level 0-to-1b processor version uses Ozone columns measured by GOME itself (from the previous GDP Level 2 data), with using the climatology only as fallback when no GOME Ozone measurement is available.

A further improvement to GomeCal may be made in the airmass calculation. In Ref. [R20], [R21] the formula for the plane-parallel case is used. This limits the calculation to solar zenith angles SZA < 85°. We use a formula for spherical geometry from H. Eskes (KNMI, private communication):

$$M = \frac{1}{\cos(VZA)} + \frac{\sqrt{\cos(SZA)^2 + (h/R)^2 + 2(h/R)} - \cos(SZA)}{h/R} \qquad \text{Eq.(6-48)}$$

where *VZA* is the nadir viewing angle, *h* is the top of atmosphere height, and *R* is the Earth radius.

This formula gives physical results for the airmass even for SZA > 90°, although the numerical values then become strongly dependent on the assumed top of atmosphere height.

We will use h = 60 and R = 6300 .

The parameters a-d in the equations above have been calculated for SZA < 75 ° and 220 < VCD < 440. We find that using our airmass calculation, these parameters still yield plausible results for SZA < 95 ° and 100 < VCD < 600 DU. There are thus no practical limitations in applying the parameters in the GDP software.

6.11.3 Polarisation correction factors

The “Calculate Atmospheric Polarisation” module, as described in Sections 6.11.1 and 6.11.2, generates a small array of fractional polarisation values at certain well-spaced wavelengths across the GOME spectral range. Up to 7 points can be specified, but since the channel overlaps are no longer used we only have 4.

Before these polarisation values can be used for polarisation correction of the measured intensity, they must be interpolated to the wavelengths of all detector pixels. The principle is illustrated in Figure 6-12.

Three polarisation points come from the comparison of channel array signals with broad-band PMD signals (in Figure 6-12 these are the filled circles at points *P* with index 1, 2, 3; the corresponding wavelengths λ_1, λ_2, λ_3 are approximately 360 nm, 500 nm and 700 nm depending on the exact spectral shape of the input spectrum). Three more points might come from the channel overlap regions (in Figure 6-12 these are the open circles at points *P* with index 4, 5, 6 for overlaps between channels 1/2, 2/3, 3/4; the corresponding wavelengths λ_4, λ_5, λ_6 are at 312.5, 400, 600 nm approximately) though these appear to be largely unusable for various reasons The last ("theoretical") point (labelled [λ_7, P_7] in the figure) comes from the Rayleigh single-scatter model simulation of polarisation in the Ultra Violet.

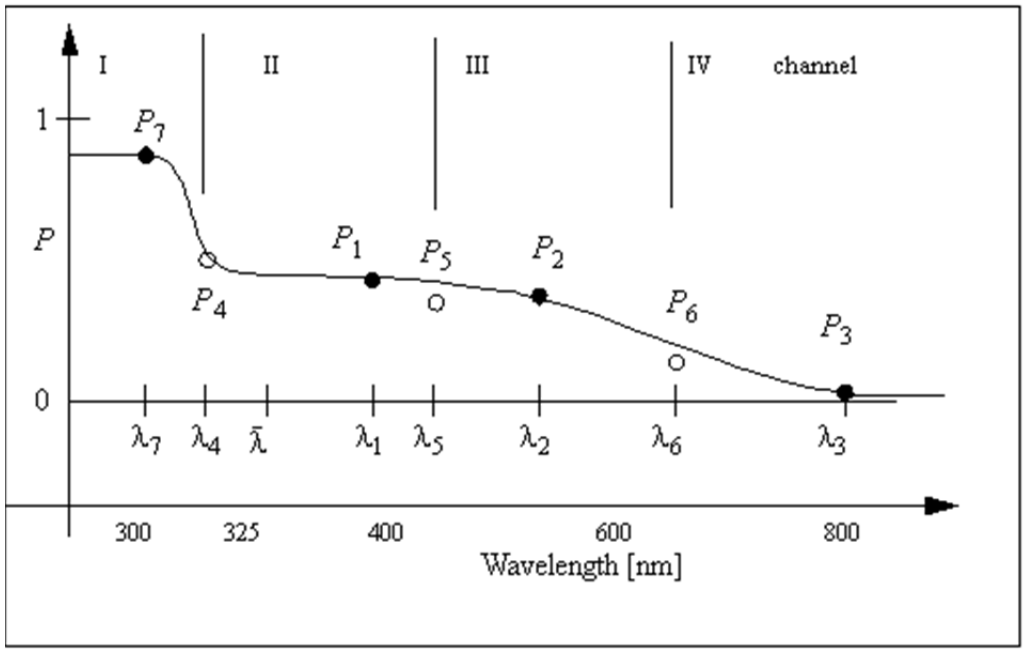

Figure 6-12 Wavelength interpolation of the polarisation points

Radiative transfer model calculations, including polarisation, have been performed by P. Stammes (KNMI) to study the polarisation behaviour in the UV for application to the GOME instrument [R7]. These simulations show that up to wavelength λ_{SS} (~300 nm, see Eq.(6-46)), the degree of polarisation $P(\lambda)$ is virtually a constant, so there we set fractional polarisation equal to the theoretical single-scatter value at $\lambda_7 = \lambda_{SS}$. $P(\lambda)$ then changes rapidly between λ_7 and $\lambda \approx 325$ nm, then shows smooth behaviour into the visible (ca. 325-400 nm). Thereafter, $P(\lambda)$ is a smooth slowly-varying function of wavelength.

The interpolation of polarisation goes basically as follows (for details see below):

- constant shortward of wavelength λ_7
- a parametrisation (see below) between λ_7 and a pre-defined wavelength (λ_7 +15 nm)
- Akima interpolation between $\bar{\lambda}$ (the end of the parametrisation) and λ_3.
- constant longward of λ_3 – this is hardcoded to 700 nm as λ_3 from Eq.(6-40) is unreliable for PMD 3 because its sensitivity extends beyond the 790 nm channel boundary.

The critical region is ~300-325 nm. An analytic function is required that mirrors the shape of simulated polarisation for all atmospheric scenarios. This function must have a turning point at the theoretical point λ_7, with parabolic fall-off behaviour near this point. The function must also show exponential tail behaviour as λ tends towards $\bar{\lambda}$. This role is fulfilled by the Generalised Distribution Function (GDF) constructed by R. Spurr:

$$P(\lambda) = \overline{P(\lambda)} + \frac{w \cdot \exp(-[\lambda - \lambda_7] \cdot \beta)}{\{1 + exp(-[\lambda - \lambda_7] \cdot \beta)\}^2} \qquad \text{Eq.(6-49)}$$

where $\{\bar{P}, w, \beta\}$ are parameters that characterise the GDF; they must be found to fit the given interpolation points.

It is noted that the actually simulated polarisation shows a bit more complex behaviour, e.g. some residual structure of the O_3 Huggins bands is visible in the polarisation (due to different airmasses in- and outside the absorption peaks with different depolarisation by aerosols), but

the approximation above was found accurate to better than 3% compared to the simulated polarisation values.

In the initial description from R. Spurr, the GDF parametrisation was maintained up to 325 nm. This results between ~320 and 325 nm in a rather flat function, and a continuous connection in gradient forces also the Akima interpolation to be pretty flat until the polarisation point from PMD-1. This behavior is not always supported by simulations of polarisation, especially above clear surfaces with low albedo (high polarisation). Here polarisation shows a local minimum near 320 nm (depending on airmass) and a local maximum near 400-450 nm.

We now use a method adapted from the SCIAMACHY ATBD [R13]. Here, the GDF parameterisation is only used between λ_{SS} and a wavelength ($\lambda_0 + \Delta\lambda_{GDF}$) which is chosen such that it falls still in the strongly descending part of the GDF (current value is set to $\Delta\lambda_{GDF}$ =15 nm). Continuation in gradient will force it to follow the GDF further downwards as would the parameterisation do, but it gives the algorithm a bit more freedom to shape the curve according to the gradient obtained from PMD measurements around λ_1.

The parameters of the GDF are calculated as follows:

- $\beta = \ln\left(2. - \sqrt{3}\right) / (\lambda_m - \lambda_7)$
- $\bar{P} = p_1$ if $(0 \le p1 \le 1)$ AND $|p7 - 0.5| \ge |p1 - 0.5|$ AND $(p7 - 0.5) * (p1 - 0.5) \ge 0$

  else $\bar{P} = (p_7 + 0.5)/2$
- $w = 4 * (p7 - \bar{P})$

The calculation of $\bar{P}$ incorporates the condition that the first PMD point is physically valid; this is the case if its value is between 0 and 1, and if the corresponding Stokes fraction Q (see Eq.(6-34)) is smaller than that of p7 and has the same sign as p7. Analysis of GOME PMD-1 data has shown that, on average, the degree of polarisation at PMD-1 is half that of the theoretical single scatter value. In case of unphysical PMD-1 values, p1 is replaced by this statistical value.

In the UV-Visible wavelength region above $\bar{\lambda}$, Akima interpolation is used. Akima [R1] is basically a spline interpolation, but with constraints to reduce overshoot. One of the benign properties of Akima compared to cubic spline, is that it doesn't oscillate when 3 subsequent points lie on a straight line. To get a smooth transition towards the GDF at short wavelengths, and to the constant value at long wavelengths, extra points are added for the interpolation. Below $\bar{\lambda}$, the channel points that lie on the GDF are added to the points at {λ_1, λ_2 , λ_3}, and above λ_3 3 points with the polarisation p3 are added, with 20 nm spacing.

Once the interpolated fractional polarisation values have been calculated, the polarisation correction factor is given by

$$c\_pol_i = \frac{1}{2} \cdot \frac{1 + \eta_i}{(1 + \eta_i) \cdot p_i + \eta_i} \qquad \text{Eq.(6-50)}$$

where subscript *i* denotes detector pixel and η incorporates the scan angle dependency.

For polarisation correction, the calibrated radiance is multiplied with this correction factor.

6.12 Determination of precision errors

In earlier processor versions (GDP 4.x and lower) the Level 1b product contained “absolute errors” in units of radiance, and “relative errors”. The “absolute error” was a precision error (see Section 8), while the “relative error” was an accuracy error, that was mainly determined by errors in the keydata.

Since this accuracy error was not very dependent on measurement, and the given keydata errors are known to be inaccurate, the accuracy error now has been dropped from the Level 1b product.

The accuracy should be estimated from geophysical validation. The precision error is now the only error provided on the Level 1b product; and now it is given as a relative error.

In the formulas, the following variables are used:

S	signal of a pixel in BU
S_e	signal of a pixel in electrons
σ_L	electronic readout and leakage current noise in electrons (for each integration time pattern)
N_e	number of electrons for 1 BU
ϵ_S	noise error on the signal in BU
ϵ_{fixed}	additional relative error due to noise from dark signal subtraction and other algorithm steps
ϵ_{Rad}	radiance precision error (noise-to-signal)
ϵ_{Irr}	irradiance precision error (noise-to-signal)

In the calculation of the leakage current (from DP_DARK measurements), a mean value of standard deviations σ_L for the dark signals of all detector pixels is determined, for each integration time pattern. If the individual detector pixel signal is denoted by *S*, then a measurement noise ε_S per pixel [BU] may be calculated :

$$\epsilon_S = \frac{1}{N_e}\sqrt{S_e + \epsilon_L^2 + \epsilon_D^2} \qquad \text{Eq.(6-51)}$$

which includes:

- the shot noise: $S_e = S \cdot N_e$
- the dark signal noise: $\epsilon_L = \sigma_L \cdot N_e$
- the digitisation effect: $\epsilon_D = 0.5 \cdot N_e$

with *Ne = 937 [electrons/BU]*

Linearity is assumed over the dynamic ranges of the detector arrays.

In the current processing, the signal is (for historic reasons) taken after correction for dark signal and PPG. This is not quite correct – signals before PPG correction should have been used, moreover the shot noise should include the dark signal whereas ϵ_L should not include the dark signal. However, the PPG effect is very small and the differences may in practice be negligible.

The radiance precision error is calculated as:

$$\epsilon_{Rad} = \frac{\epsilon_S}{S} + \epsilon_{fixed} \qquad \text{Eq.(6-52)}$$

The term ε_{fixed} accounts for noise introduced by dark signal subtraction, PPG errors, and interpolation noise from regridding the radiance keydata to the actual wavelength grid. It is set to an estimated value of 3.e–4 .

The precision error on the solar irradiance is similarly given by:

$$\epsilon_{Irr} = \frac{\sqrt{\sum_n (\epsilon_S)^2}}{\sum_n S} + \epsilon_{fixed} \qquad \text{Eq.(6-53)}$$

where n denotes index over measurement in the solar calibration sequence.

6.13 Quality flagging

Currently only two quality flags are set in the Level 1b product:

- saturated pixels: the raw measurements [BU] exceed a limiting level
- negative values: calibrated radiances are < 0

The pixel flag for saturated readouts is set, when the [raw] detector signals exceed a limit of 52926 , 55849 , 52519 , 55836 BU (hardcoded values) for channels 1,2,3,4 respectively.

The pixel flag “other” is set for negative calibrated radiances.

Further pixel flags on the Level 1b product are “dead” and “hot”, but these are currently unused (placeholders). In the future, they might be set depending on PPG threshold values.

7 Algorithm Limitations

Limitations of the Radiance Calibration

- Errors due to shifts in spectral structure of the etalon effect are not corrected. This should not be a problem for sun-normalised spectra, but an etalon-like structure with amplitudes of up to a few percent may be visible in radiance (Earth, Moon) or irradiance (Sun) spectra.
- It is known that, especially in channel 3, the on-ground calibration determination of η was not very accurate due to outgassing problems with the dichroic, leading to issues with polarisation correction. This issue is still present for Keydata version 8.
- In Keydata version 8, "noise" can be seen on the calibration parameter η which may or may not be a real structure. If it were noise, it will be aliased into the calibrated radiance, and could adversely influence the pixel-to-pixel precision of the measurements for high values of the atmospheric polarisation.
- Errors in the determination of polarisation fraction *p*, or in the wavelength interpolation of *p,* may lead to spectral features in the spectrum (features reflecting the spectral shape of keydata η).
- The calculation of polarisation fraction *p* from PMDs is not entirely self-consistent (as *p* is first approximated constant over the PMD band and then centre points are interpolated in wavelength) , also the extrapolation of *p* with a constant beyond 700 nm is not ideal. Experimental methods for improvement have been derived by N. Schutgens, but this needs characterisation of the surface albedo and would bring more theory into the polarisation correction.
- The polarisation correction assumes that atmospheric polarisation is a smooth function of wavelength. However, it is known that in strong atmospheric absorption lines (especially the O_2-A band but also the O_3 Huggins bands) polarisation in the line may be different from the continuum. Neglecting line polarisation may affect the measured line absorption depth.

Limitations of the Degradation Correction

- no scan-angle dependency is taken into account
- In the calculation of polarisation from PMDs, degradation is taken into account lump-sum through the correction factor Q_{SUN}. It would be better to correct signals for degradation before they are used in the Virtual Sum, since keydata ξ and η are valid for non-degraded measurements (however, as long as the degradation correction does not take scan angle dependence into account, its effect on ξ may not be significant).
  The reason that this improvement is not made yet, is that it would significantly change the processing flow in order to obtain consistent database entries for Q_{SUN}.

Limitations of the L1b Data Product

- Measurements from the DP_LAMP_DIFFUSER list are currently not used operationally and not available to external users. It may be considered to write average lamp+diffuser spectra (for each temperature) to the L1b product
- Measurements from the DP_LAMP list are not available to end users. It may be considered to write averaged lamp spectra (for each temperature) to the L1b product
- There is currently no flagging of bad pixels

8 APPENDIX: General description of errors

Two major types of error which are determined during the Level 0 to 1 Processing, are:

1. Wavelength errors – the uncertainty on the spectral calibration parameters; and
2. Radiometric errors – the relative/absolute errors on the radiance and irradiance measurements.

The wavelength errors are determined from the polynomial fitting of the spectral calibration parameters from lamp line centroid–pixel/wavelength pairs; these fitting errors are archived in the in-flight calibration database. Radiometric errors are calculated during Level 0-to-1b processing for each individual detector pixel and written to the output product.

8.1.1 Prerequisites

The following sources of errors may be distinguished for GOME measurements:

Coarse Errors

These errors are severe deviations from expected results. They occur for internally or externally caused instrument failures or wrong handling of the instrument. There is no precise rule or mathematical description for such errors. Although careful and comprehensive measurement procedures should eliminate most coarse errors, chance events can occur to produce unavoidable gross errors. It is then necessary to identify the measurement as 'wrong', and either reject it or try to correct it with an appropriate model. A "hot" detector pixel is an example of a coarse error source.

Systematic Errors

Systematic errors are expected deviations from the true values of a measurement that may be described with a physical model. It is the major objective of every calibration activity to take these physical laws into account and correct for such kind of measurement errors. There are three types of systematic errors:

– Static Errors due to a known constant bias or a known functional dependence of the measurements with respect to the physical parameter in question (e.g. linear function of the temperature sensors);

– Drift Errors caused by long–term changes of parameters (e.g. warming of the optical bench during the lifetime of the sensor);

– Periodic Errors are similar to drift errors, but the changes of certain parameters are periodic (e.g. temperature change during orbit; etalon structures)

The application of physical rules to estimate systematic errors requires the ancillary measurement of relevant physical values (e.g. temperature) and/or the use of appropriate models. As these other values and models are also not free of errors, and the propagation of any such additional errors must be accounted for. One can say that the in–flight calibration activities of the GOME sensor are mainly the correction for systematic errors – this must include the propagation of errors on the correction factors throughout the calibration algorithms.

Random Errors

Random errors on measurements are caused by known physical effects, but by their nature are unpredictable in size and direction. Normally these errors are the so–called noise; this should be as low as possible compared to the measurement signal. During the design phase, the signal to noise level (S/N) is one of the most important performance criteria by which the quality of the instrument can be properly assessed.

Random errors can only be analysed by statistical methods. Single measurements cannot be corrected for random errors; a sample of measurements (sample size ideally > 10) taken under the same conditions is needed to compute mean values, standard deviations and other statistics. statistical algorithms like mean value, standard deviations, etc. If such samples are not available, noise levels should be characterised during a calibration exercise in order to assign error bars to individual measurements.

It is important to distinguish between the terms ***accuracy*** and ***precision***:

- The *accuracy* of a measurement is a measure of how close its result is to the true value.
- The *precision* of a measurement is a measure of how well its result has been determined, without reference to its agreement with the true value. Precision is therefore a measure of the reproducibility of the result.

Assessment of Random Errors

If x is the true value and a the result of one measurement of x, the true error ε^{true} of this measurement is defined to be:

$$\in^{true} = a - \chi$$

If x is unknown, so also is ε^{true}. From a statistical sample of similar measurements, an approximate value μ for x and its probability boundaries ±σ can be derived.

If these measurements are given by $a_1, a_2, a_3, \ldots, a_n$ the statistical parameters are:

$$\mu = \frac{1}{n} \cdot \sum_{i=1}^{n} a_i$$

$$\sigma = \sqrt{\frac{1}{n} \cdot \sum_{i=1}^{n} (a_i - \mu)^2}$$

With the approximate value μ in place of the unknown true value x, the approximate error ε_i of each individual measurement a_i is:

$$\in_i = a_i - \mu$$

The estimated error ε_μ of the mean value μ of a measurement series is given as follows:

$$\in_\mu = \frac{1}{n} \cdot \sqrt{\sum_{i=1}^{n} \in_i^2} = \frac{\sigma}{\sqrt{n}}$$

In most cases, the measurement value is assumed to be Gaussian Normal Distributed, with the probability density function Φ characterised by the parameters μ and σ :

$$\phi(a) = \frac{1}{\sigma\sqrt{2\pi}} \cdot e^{-\frac{(a-\mu)^2}{2\sigma^2}}$$

Thus the probability P that the measurement a of a parameter x will lie between certain boundaries (±Δ) is given by:

$$P = \int_{\mu-\Delta}^{\mu+\Delta} \Phi(a) da$$

Some typical and useful values of P are given in the following table:

Boundary Δ	Probability P
0.67σ	0.500
1.00σ	0.683
1.96σ	0.950
2.00σ	0.954
2.58σ	0.990
3.00σ	0.997

In what follows, error calculations will use 1σ as error boundary to express the relative errors.

Error Propagation

GOME data is converted into ”calibrated radiances” by applying calibration algorithms and calibration parameters. Many calibration parameters are established on a regular basis from in–flight observations of the calibration lamp, the internal LED and the sun and under dark conditions. In addition, data from pre–flight instrument calibration and characterisation (e.g. the polarisation characteristics of the optical chain) is required. All of these calibration parameters have errors. The size and type of errors on the pre–flight calibration parameters has been estimated in [G4].

During the calculation and application of the calibration parameters, a number of formulae are used to determine intermediate and the final results. In the GDP level 0 to 1 processing chain, the propagation of the errors through these formulae to the end results are done by means of the Gaussian Error Propagation Law. If

f(x1 , x2 , x3 , ..., xn)

is a function of the values x1 , x2 , x3 , ..., xn and ε1, ε2, ε3, ...,εn are the corresponding approximated errors of these values, the error on the function result is defined as follows:

$$\in = \sqrt{\left(\frac{\partial f(x_1, \ldots, x_n)}{\partial x_1}\right)^2 \cdot \in_1^2 + \ldots + \left(\frac{\partial f(x_1, \ldots, x_n)}{\partial x_n}\right)^2 \cdot \in_n^2}$$

For addition, multiplication and division of two parameters, this has the following effect:

$$f(x_1, x_2) = x_1 + x_2 \qquad \in = \sqrt{\in_1^2 + \in_2^2}$$

$$f(x_1, x_2) = x_1 \cdot x_2 \qquad \in = \sqrt{x_2^2 \in_1^2 + x_1^2 \in_2^2}$$

$$f(x_1, x_2) = \frac{x_1}{x_2} \qquad \in = \sqrt{\left(\frac{1}{x_2}\right)^2 \in_1^2 + \left(\frac{-x_1}{x_2^2}\right)^2 \in_2^2}$$

8.1.2 Wavelength Uncertainty

In the calculation of the spectral calibration parameters, the ’fractional’ pixel number of a selected lamp line is determined as a statistical signal mean value, and the spectral calibration coefficients come from the linear fitting of a polynomial to a selected number of pixel number/wavelength pairs.

The estimated deviation of the wavelength for each detector array is:

$$\in_\lambda = \frac{\frac{1}{k} \cdot \sum_k \in_i}{\sqrt{k - f}}$$

where k is the number of lines used in the fit, f is the degree of freedom of the fitted polynomial and:

$$\epsilon_i = |\lambda_{lit} - \lambda_i|$$

(literature wavelength minus calculated wavelength)

If ε_i is divided by the linear coefficient of the spectral calibration parameters, the error is given in detector pixels.

8.1.3 Radiometric Errors

Unfortunately, the assessment of the radiometric errors is much more complicated. Several corrections are applied to the raw signal values using pre–flight and in–flight calibration parameters; all such processes will propagate parameter errors to the final result. The following errors on the radiometric signals are present.

- calculation of leakage current noise (includes electronic/readout noise and digitisation effects)
- calculation of photon shot noise induced by incident light
- estimation of the error on the fractional polarisation values
- calculation of the error on the polarisation correction factor

The first two items comprise the *precision* of the radiance measurements done with GOME, while the second two error sources contribute to the *accuracy* of the measurements.

In addition, the following error sources are also required for the accuracy calculation of GOME measurements:

- error on the BSDF
- error on the radiance sensitivity
- error on the polarisation sensitivity

In earlier document versions, a rigorous mathematical description of the accuracy was given, based on errors to be taken from the error budget analysis of TPD for the pre–flight calibration parameters. For reasons given in Section 6.12, this accuracy calculation has been dropped for product generation.